Optimization of Nickel Oxide/FTO based HTL Thin Films for Solar Cell Applications

By

Seemin Fatima

School of Chemical and Materials Engineering

National University of Sciences and Technology

2023

Optimization of Nickel Oxide/FTO based HTL Thin Films for Solar Cell Applications

Seemin Fatima

Reg.No:00000320663

This thesis is submitted as a partial fulfillment of the requirements for the degree of

"Master of Science (MS) in Nanoscience and Technology"

Supervisor Name: Dr. Muhammad Talha Masood

School of Chemical and Materials Engineering (SCME)

National University of Sciences and Technology (NUST)

H-12 Islamabad, Pakistan

July, 2023

THESIS ACCEPTANCE CERTIFICATE

Certified that final copy of MS thesis written by Ms **Seemin Fatima** (Registration No 00000320663), of School of Chemical & Materials Engineering (SCME) has been vetted by undersigned, found complete in all respects as per NUST Statues/Regulations, is free of plagiarism, errors, and mistakes and is accepted as partial fulfillment for award of MS degree. It is further certified that necessary amendments as pointed out by GEC members of the scholar have also been incorporated in the said thesis.

Signature: _____

Assistant Professor
School of Chemical and
Materials Engineering (SCME)
NUST, Islamabad (Pakistan)

Name of Supervisor: **Dr Muhammad Talha Masood**

Date: 05/09/2023

Signature (HOD): _____

Date: 11/09/23

Signature (Dean/Principal): _____

Date: 11.9.2023

National University of Sciences & Technology (NUST)

MASTER'S THESIS WORK

Formulation of Guidance and Examination Committee (GEC)

Name: Seemin Fatima   NUST Regn No: 00000320663

Department: SCME   Specialization: MS Nanoscience And Engineering

Credit Hour Completed: 24   CGPA: 3.56

Course Work Completed

S/No	Code	Title	Core/Elective	CH	Grade
1	NSE-845	Nanolithography And Device Fabrication	Elective	3	B+
2	MSE-854	Characterization Of Materials	Core	3	B+
3	NSE-813	Essentials of Nanoscience And Engineering	Core	3	B+
4	MSE-856	Nano Material And Processing	Core	3	B+
5	MSE-862	Electronic And Magnetic Materials	Elective	3	B+
6	MSE-872	Composite Materials	Elective	3	B+
7	MSE-952	Materials For Biomedical Applications	Elective	3	A
8	NSE-941	Nano Composite Materials	Elective	3	B+

Date 9 July 2021   Student's Signature

Thesis Committee

1. Name: Dr. Muhammad Talha Masood   **(Supervisor)**
    Signature:
    Department: SCME

2. Name: Dr. Sofia Javed   **(Co-Supervisor, if appointed)**
    Signature:
    Department: SCME

3. Name: Dr. Zakir Hussain
    Signature:
    Department: SCME

4. Name: Dr. Aftab Akram
    Signature:
    Department: SCME

6. Name: Dr. Muhammad Siyar
    Signature:
    Department: SCME

Date: 31/8/2021   Signature of Head of Department:

APPROVAL

Date: 31. 8. 2021   _____
                         Dean/Principal

School of Chemical and Materials Engineering (SCME) Sector H-12, Islamabad

National University of Sciences &Technology (NUST)

FORM TH-4

MASTER'S THESIS WORK

We hereby recommend that the dissertation prepared under our supervision by

Regn No & Name: **0000320663 Seemin Fatima**

Title: **Optimization of Nickel Oxide Thin Films as Hole Selective Layer for Photovoltaic Applications.**

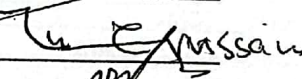Presented on: **30 Aug 2023**   at: **1430 hrs in SCME Seminar Hall**

Be accepted in partial fulfillment of the requirements for the award of Masters of Science degree in **Nanoscience & Engineering.**

Guidance & Examination Committee Members
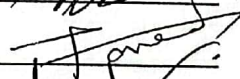
Name: **Dr Muhammad Siyar**   Signature: _____

Name: **Dr Zakir Hussain**   Signature: _____

Name: **Dr M. Aftab Akram**   Signature: _____

Name: **Dr Sofia Javed** (Co-Supervisor)   Signature: _____

Supervisor's Name: **Dr M. Talha Masood**   Signature: _____

                                          Dated: 30/08/2023

_____   _____ 4.9-2023

Head of Department   **Dean/Principal**

Date _31/08/2023_   Date ___4.9.2023___

School of Chemical &Materials Engineering (SCME)

Dedication

This thesis is dedicated to my parents and my husband for their love, support, sacrifices, prayers, and advice.

Acknowledgments

Abstract

In this research study, compact Nickel oxide (NiO) thin films were studied for their potential application as hole selective layers (HSL) in perovskite solar cells (PSCs). The films were deposited on top of Fluorine doped Tin Oxide (FTO) coated conductive glass substrates. Different thin film deposition techniques were used including spin coating, electrodeposition, and dip coating. However, dip-coating was preferred during most of this research work because of good surface coverage and film uniformity as compared to electrodeposition and spin coating. The dip-coating is a scalable solution-processable thin film deposition technique thus, it is a simple and economical route towards shifting from lab-scale devices to large-sized commercial PSCs. In this research study, the dip coating was performed under ambient conditions using 85 mm/min withdrawal speed. 0.5M solution of $NiAc_2.4H_2O$ dissolved in ethanol was used as a precursor solution. After drying and calcination, the films were characterized using Raman, XRD, EDS and UV-Vis spectroscopy to confirm the successful synthesis of NiO films. The optical profilometry was used to investigate the variation in film thickness as a function of dipping time. Cyclic Voltammetry (CV) revealed that the reaction activity of the NiO thin film increases with time and uniformity. The influence of plasma treatment prior to the dip-coating procedure was studied against the optical and electrical properties of the NiO thin films. One of the important observations during this research work indicated that plasma treatment tends to enhance transmittance of NiO thin films due to increase in their band gap and increased surface coverage.

Table of Contents

List of Figures

List of Tables

Chapter 1

Introduction

Electricity is an important part of our daily life. However, conventional electricity generation and transmission processes are highly dependent upon complex and high-cost infrastructure (such as hydroelectric power stations and high-tension cables). Using fossil fuels for this purpose pose significant threat to our environment. Therefore, extensive research is being carried out by the scientific community to shift towards renewable energy resources. One such energy resource is our sun which exists in the heart of our solar system. Solar energy comprises of a large portion of visible and infrared radiation along with 5% UV portion of the electromagnetic spectrum. Converting this freely available energy into electricity requires photovoltaic technology which has already penetrated well into the market. The photovoltaic devices are also called solar cells and they generally comprise of conventional P-N junction Silicon devices. However, there are a variety of materials for their potential use in photovoltaic technology which are still in research phase today. The technology that generates power from visible light is known as solar cells. These cells are particularly important since they generate electricity from renewable resources, in this case the sun. These cells have made use of a variety of materials.

The solar cells have been categorized into three different generations. A device being from the latest generation does not necessarily means an all-round better device from the previous ones. However, this categorization approach is based on device structure and the kind of materials involved in solar cell manufacturing.

The first-generation solar cells were formally introduced in early 1950s in the form of P-N junction Silicon diodes for space technology applications. Now they are widely being used for different application across the globe. They are technologically advanced and highly stable. In Pakistan, India and other south Asian countries, they are being extensively used for domestic and agricultural applications (for instance, to power tube-wells for irrigation). To reduce the cost and the amount of material use, second generation solar cells were introduced. With the passage of time, thin-films

(also known as third generation) solar cells were introduced to further reduce the cost and material usage in final device. Almost every third generation is in research phase.

The significance of charge transport layers has been established by many device topologies. Perovskite Solar Cells (PSCs) are a type of solar cell that has thus demonstrated extraordinarily high efficiency. These PSCs represent the apex of current research trends. The absorber layer, charge transport layers (the electron and hole transport layers), back and front contacts, and all the other layers are therefore present in PSCs device topologies [1].

In perovskite solar cells (PSCs), the Hole Transport Layer (HTL) is important for efficiently extracting holes from the perovskite film and transporting them to the metal electrode. Nonetheless, the focus of this research is on only ETMs and will be discussed in detail in this chapter [2].

1.1. Hole Transport Materials (HTM)

HTMs are an important component in the perovskite solar devices. The extraction and transportation of positive charges (holes) produced by the absorption of light are greatly aided in perovskite solar cells by the hole transport layer (HTL). It is located between the top electrode, which is typically constructed of a transparent conducting oxide (TCO) like indium tin oxide (ITO), and the perovskite active layer.

Some of the key requirements for HTMs are as follows:

- Hole Extraction: After the perovskite layer has absorbed light, electron-hole pairs (excitons) are produced. To effectively remove these holes from the perovskite layer and stop them from recombining with electrons, the HTL acts as an interface.

- Charge Transport: The HTL makes it possible for the extracted holes to be transported quickly and effectively towards the top electrode. To reduce carrier losses and promote effective charge collection, this layer should have high hole mobility.[3]

- Energy-Level Alignment: The HTL aids in aligning the energies between the top electrode and the perovskite layer. This alignment helps to reduce energy barriers that could obstruct charge transit and achieve effective charge extraction.[4]

The instability and/or negative impacts of the organic hole transport layers (HTLs) are one of the potential causes of the PVSCs' instability. NiO HTL facilitates the production of thick, high-quality perovskite films by having a sufficient energy level with perovskite, good optical transparency in the visible region, and high stability. NiO derivatives were chosen to accomplish our goal because of their broad band gap (about 3.6 eV), deep valance band edge (about 5.4 eV) [5], simplicity of altering composition, low cost, and excellent thermal and chemical stabilities. In reality, NiO-based HTLs have been utilised to create inverted and other types of PVSCs, and studies about them have frequently focused on the stability problem. Fluorine-doped tin oxide (FTO) has a significant surface roughness, which has so far prevented it from being widely used in PSCs. However, the surface roughness can be reduced by surface modification of FTO. Oxygen plasma treatment creates reactive species such as oxygen radicals which react with material's surface resulting in the formation of various functional groups. These functional groups offer additional reactive sites for chemical bonding, enhancing the adhesion of NiO coatings. We employed Oxygen plasma treatment to modify the surface. This improved the compactness and homogeneity of NiO thin films on FTO substrate. [6]

1.2. Objectives

The objectives of this research study are listed as follows:

- To compare NiO thin-films prepared using different solution-processable techniques (i.e., spin-coating, electrodeposition and dip-coating).
- Choosing the most optimal technique for further processing (which later came out to be dip-coating route).
- To compare structural, morphological, and optical properties for samples prepared with and without plasma activation.
- To compare the electronic properties (using Hall-effect approach) for samples prepared with and without plasma activation.

Chapter 2

Literature Review

2.1. Solar Cells

Solar cells are devices that produce electron-hole pairs through photon absorption by the sun. This along with basics of solar irradiation is discussed in this section.

2.1.1. Motivation

The global need for energy is continuously rising. Future increases in energy demand will occur at an alarming rate due to the recent boom in worldwide population growth. This increase can be linked to the high-tech electronics and industrial revolutions as well as the population growth rate. Humanity is now more dependent on energy than ever before, and this dependence will only grow as a result of the expected futuristic development.

The world's population has greatly increased; it is currently projected to number around 7.5 billion people (Fig. 2.1) [3]. Resources are needed to meet the population's energy demands. By using up all of the fossil fuels, which are already scarce, this was being accomplished. Fossil fuels are also unsustainable, which implies that CO_2 emissions occur during these processes. Particularly because it alters the climate, this is a problem. As a result, developing nations are looking for fresh and cutting-edge energy sources [4, 5].
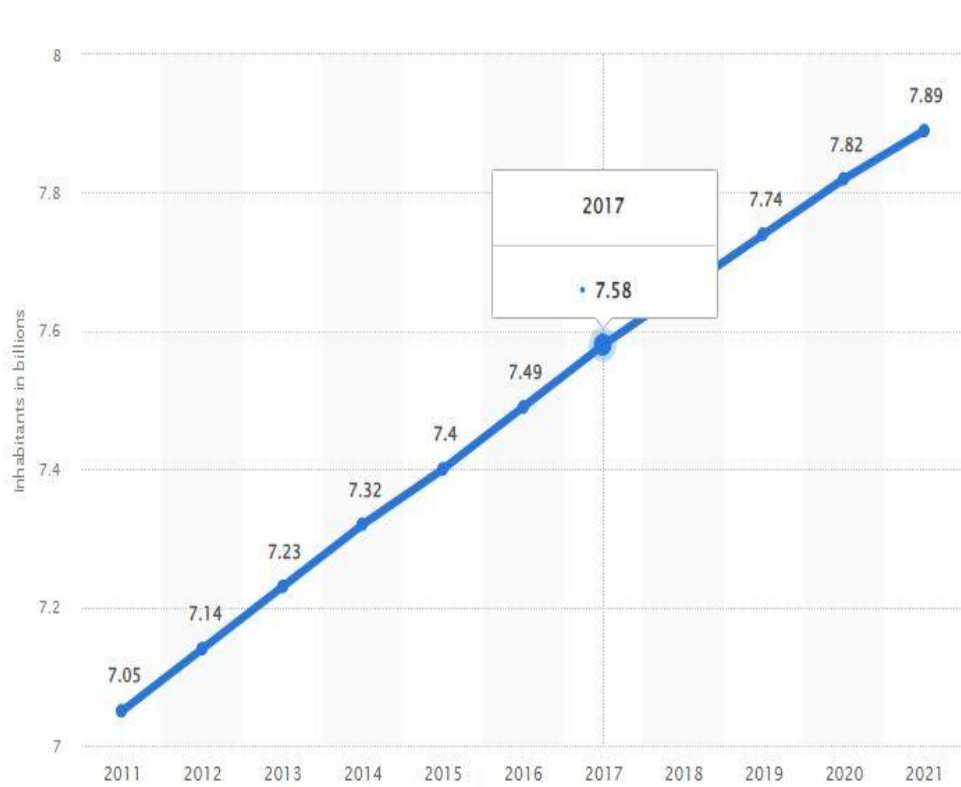
Figure 2. 1. World Population Estimated Statistics [4]

The new and creative methods of energy production are significantly more environmentally friendly and are a superior option for a number of reasons. Environmentally friendly practices affect ecosystems less and make climate change more manageable. These environmentally friendly energy sources could include hydropower, geothermal energy, solar and wind energy and solar energy [6].
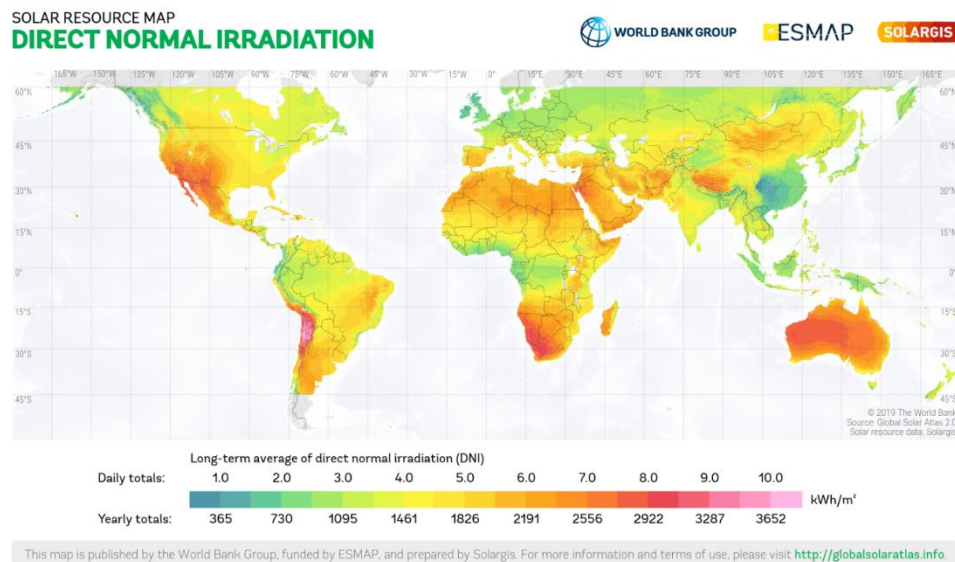
Figure 2. 2. Global Map of Horizontal Irradiation [7]

5

Solar energy is viewed as a leading possibility to meet future energy needs since it has a number of benefits over other renewable and environmentally acceptable energies. First off, the sun is a plentiful source of energy in nature (Fig. 2.2). Additionally, it is free, in contrast to fuels made of fossils. On average, 1.8 1014 kW of solar energy from the sun is intercepted on earth [8].

The development of solar energy technologies has made it possible to access the enormous potential of solar energy. The recent development of nanotechnology has increased the range of options. Nanotechnology is already being used to develop novel and creative solutions, and it has already shown encouraging signs in terms of improving productivity, reproducibility, longevity, and stability. Therefore, one must take advantage of such opportunities to address future energy needs [9, 10]

2.1.2. Overview

Through photovoltaics, solar energy is transformed into electricity that may either be utilized immediately or stored in batteries. These photovoltaics, often known as solar cells, are power producing systems. These cells come in a variety of forms, and as a result, they are divided into generations, each of which has unique advantages, drawbacks, and historical significance. Every generation of solar cells has conquered its own obstacles and produced positive outcomes [11].

A half-century ago, the first Solar Cell generation was created. These days, they operate efficiently. However, there is a flaw with this generation of solar cells. They are expensive and difficult to produce. While the second generation of solar cells has essentially overcome the difficulties that its predecessor experienced, efficiency was sacrificed in order to do so. The third generation was created in order to actually attain good efficiency.

Although they have produced some encouraging outcomes, they are still in the research stage [12, 13]

Over the past few years, tremendous advancements in nanoscience and nanotechnology have been made. In order to further improve the current systems and gadgets, great strides have been made in incorporating new ideas employing nanotechnology.

In addition to improving many properties, nanoscience has forced the scientific community to reconsider old ideas. The third generation of solar cells has utilised nanoscience and nanotechnology, which has significantly improved significant features while reducing costs and efficiencies [14].

Perovskite solar cells could be one of the third generation of solar cell types.

Perovskite structure serves as the light-absorbing component of perovskite solar cells, as the name suggests. On either side of the light absorber material in such cells are electron transport materials (ETMs) and hole transport materials (HTMs).

All aspects of perovskite solar cells are being researched, and fresh findings are released every week in an effort to increase efficiency, stability, and cost effectiveness. As a result, this research has been done using nanotechnology and focuses on one element of HTMs [15].

2.2. Working of a Solar cell

A basic solar cell, commonly referred to as a photovoltaic cell, deals with solar light energy and transforms it into an electric current. The photo-sensitive substance absorbs a photon from the sun, which then produces an exciton. The creation of electron-hole pairs is referred to as an exciton. The electron is compelled to move to a higher energy state when this is formed. The electron is then forced to enter the outer circuit as a result. The energy produced by the photon is lost by the electron once it enters the outer circuit (Fig. 2.3) [16].
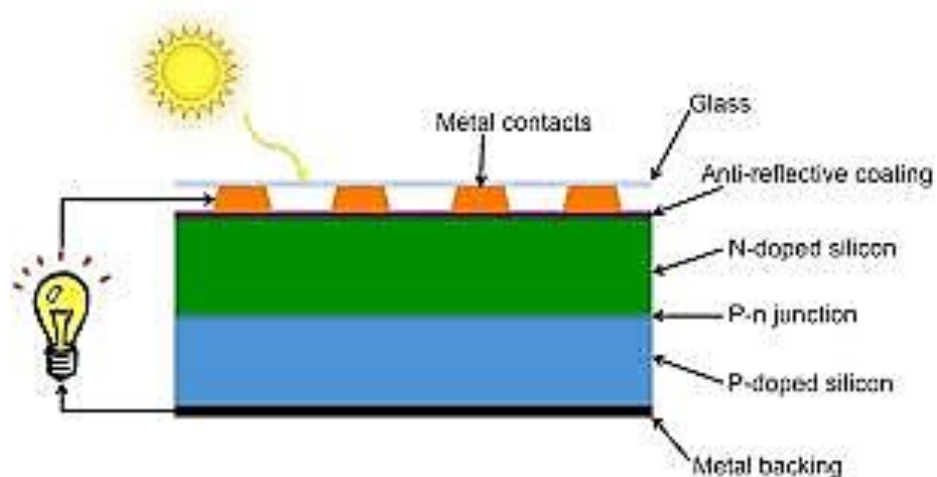
Figure 2. 3. Basic Photovoltaic Cell [16]

Solar cells are divided into different categories according to the materials they are made of.

Due to their special uses, these materials are categorised into three generations of solar cells.

- First Generation of Solar Cell
- Second Generation of Solar Cell
- Third Generation of Solar Cell

2.2.1. First generation Solar Cells

Silicon was the only known substance utilised to create solar cells when they were created for the first time. Silicon is not a component of the solar cell itself. It is doped to become a p-type and n-type material by adding either boron or phosphorus. These, in turn, utilised to create a p-n junction in a solar cell. As a result, this kind of solar cell is well-commercialized. These solar cells are pricey to create and have very poor efficiency when compared to their production costs. Such solar cells are capable of efficiency of up to 25% [17].

Figure 2. 4. Multi-Crystalline Silicon Solar Cell panel [17]

2.2.2. Second generation Solar Cells

Such solar cells are frequently related to thin-films. The second generation consists primarily of thin films produced using chemical and physical vapour deposition techniques. As a result, compared to its predecessors, the production costs are significantly cheaper. Because of this, these solar cells are less expensive yet have lower efficiency. The stated efficiencies for second-generation solar cells typically

range between 12 and 20%. Amorphous Silicon, Cadmium Sulphide, Cadmium Telluride, and Cu-In-Ga-Se (CIGS) are among the materials employed [18].
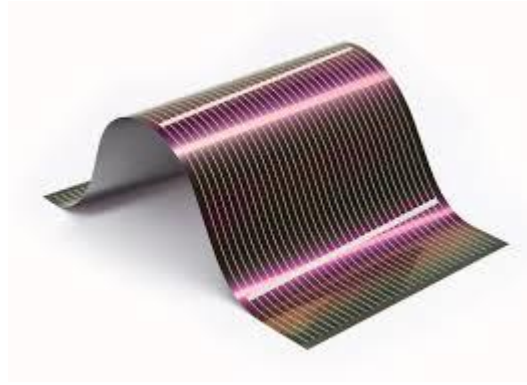
Figure 2. 5. Thin-Film Solar Cell

2.2.3. Third generation Solar Cells

Solvent processing is possible with solar cells of this generation. As a result, both chemical and physical methods of manufacture are taken into account while creating these kinds of solar cells.

Third generation's fabrication processes are substantially different because they incorporate nanomaterials. A crucial issue to take into account. As a result, the high efficiency levels are maintained while maintaining the cheap cost of production. The efficiencies range from 12 to 23% and are equivalent to single crystal silicon cells. Thus, despite relatively limited commercialization, research is still being done on the third generation of solar cells.

This generation of solar cells also includes a variety of solar cell types, such as the dye-sensitized solar cell (DSSC), quantum dot cells, organic solar cells, and perovskite solar cells, among others [19].
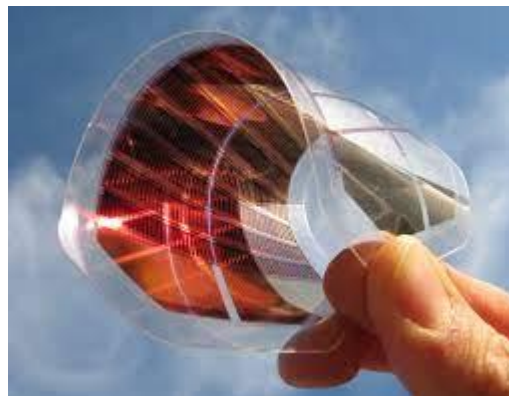
Figure 2. 6. Organic solar cell [20].

2.2.4. Perovskite Solar Cells

As the name implies, perovskite solar cells are made of materials with this structure. These structures are composed of hybrid cations and anion that are both organic and inorganic. The abbreviated formula is ABX3, where X is an anion and A and B are cations (A is bigger than B). In this context, X denotes a halogen anion typically made up of iodine, bromine, or chlorine, while A denotes an organic cation made up of either methylammonium (CH3NH3 +) or formamidinium (NH2CHNH2 +), and B denotes the cations lead (Pb) and tin (Sn).
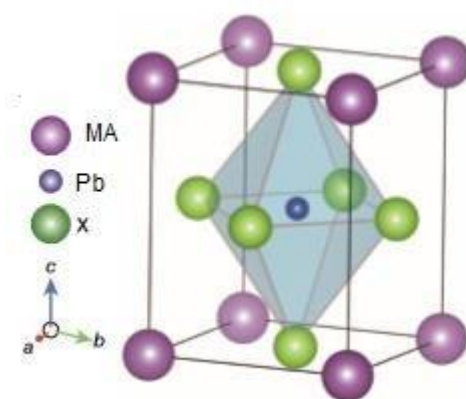
Figure 2. 7. Methyl-Ammonium Lead Iodide structural model [21]

The fundamental characteristics of such cells include their ease of manufacture, high solar spectrum absorption, and significantly lower carrier recombination rates. These materials are easily fabricated using solution processing techniques. However, the toxicity of Pb, which is frequently employed, is a drawback of perovskites. The stability factor, which is also an attribute, is one that is currently the subject of in-depth research. A glass substrate covered in transparent conducting oxide (TCO), electron transport materials (ETMs), a photoactive layer consisting of perovskite materials, hole transport materials (HTMs), and gold back contacts make up the structure of the cell. The photoactive layer is reached by sunlight passing through TCO and ETMs, where photons cause exciton to be produced. Excitons are then used by HTMs and ETMs to create current.[23]

Figure 2. 8. Inverted Perovskite Solar Cell Device architecture [22]

2.3. Nanoscience & Nanotechnology

Materials with one or more dimensions between 1 and 100 nm are referred to as nanomaterials. The characteristics of the nanomaterials vary greatly compared to their bulk or microscopic equivalents. This is because the surface-to-volume ratio has increased, which means that the number of atoms on the surface has increased.

As it increases the size is shrunk in either one or more dimensions, compared to the volume of the nanomaterials. Electronic conductivity improves where there are fewer flaws due to the increase in surface atoms. Additionally, the attributes of band gap, mechanical, thermal, and chemical reactivity all show an improvement.

2.3.1. Types of nanomaterials

Nanomaterials can be classified based on their dimensions and are of four types.

- Zero Dimensional (0-D)
- One Dimensional (1-D)
- Two Dimensional (2-D)
- Three Dimensional (3-D)

2.3.1.1. Zero Dimensional (0-D)

These types of materials characteristically have all their dimensions in the nanometer scale range of 1nm-100nm. Such materials comprise of nanoparticles (NPs), quantum dots, etc

2.3.1.2. One Dimensional (1-D)

These types of materials characteristically have one dimension outside the nanometer scale range. Such materials consist of nanotubes, nanorods, nanowires, etc.

2.3.1.3. Two Dimensional (2-D)

These types of materials characteristically have two dimensions outside the nanometer scale range. Such materials cover nanoplatelets, nanosheets, thin films, etc.

2.3.1.4. Three Dimensional (3-D)

These types of materials typically have all three dimensions outside the nanometer scale range. Such materials are also called bulk materials as their dimensions exceed the nanometer scale ranges [23].

2.3.2. Synthesis techniques

Various synthesis techniques involving spin coating, electro deposition and dip coating were used in order to achieve NiO thin films.

2.3.2.1 Principle:

Spin coating is the application of a liquid suspension or solution to a spinning substrate. Due to the interaction of rotating speed, solution viscosity, and solvent evaporation, centrifugal force distributes the liquid into a thin and homogeneous film. Electrodeposition: Electrodeposition, commonly referred to as electroplating, is the process of depositing metal or other materials onto a conductive substrate by means of an electric current. The chosen material is deposited onto the substrate by adjusting the electric potential and current while it is submerged in an electrolyte solution [24].

Dip coating is submerging a substrate in a liquid solution or suspension and then gradually pulling it out. The liquid sticks to the substrate's surface as it is removed, and any extra liquid drains off, leaving behind a coating [25].

Slides obtained by all three methods were examined by SEM to inquire about the coating with maximum homogeneity and uniform coverage.

Dip coating method was chosen for this research due to the following reasons:

- It provided maximum uniformity.
- It is most suitable for large scale manufacturing of solar cells [26].

2.3.2.2. Why not use spin coating or electro deposition?

The aim of this research is to produce films with good uniformity and adapt a procedure which can be utilized in big scale manufacturing. Spin coating is good for laboratory scale preparation but isn't the best choice for industry because:

1. Material waste: Spin coating is the process of putting a liquid solution on a rotating substrate, which causes the solution to spread out as a result of centrifugal force. Usually, the extra material is spun off and wasted. Due to the enormous material waste produced by this technology, large-scale production is not economically feasible [27].

2. Limited substrate size and shape: Because of the centrifugal force required, spin coating works best on flat, tiny substrates. It becomes difficult to scale up the process to larger substrates or complex geometries, and this frequently leads to non-uniform coating thickness [28].

3. Inaccurate control of film thickness: In spin coating, it can be challenging to achieve accurate control over the film thickness. The resulting film thickness can be influenced by variables like spin speed, solution viscosity, and solvent evaporation rate. In high-volume manufacturing, it is difficult to reliably manage these factors, which causes differences in product quality [29].

4. Slow production rate: The spinning of the substrate at a controlled speed while waiting for the liquid to spread and evaporate makes spin coating a relatively slow operation. It is not appropriate for high-throughput manufacturing because the time it takes for the coating to dry restricts the production pace [30].

Moreover, film deposited through spin coating showed less uniformity to that compared to that produced by dip coating.

A layer is deposited onto a substrate via the electro deposition technique, sometimes referred to as electroplating. Although electrodeposition is frequently used for many different purposes, there are a few drawbacks that occasionally render it unsuitable for high-scale manufacture. Here are some of the causes:

1. Limited deposition rate: Electrodeposition is a relatively slow process compared to other manufacturing techniques, especially when depositing thicker layers of metal. This can result in low productivity and longer manufacturing times, making it impractical for high-volume production.

2. Batch processing: Electrodeposition is typically a batch process where a limited number of parts can be plated at once. This makes it challenging to achieve high throughput required for large-scale manufacturing. Continuous or inline processing methods are often more efficient for high-volume production.

3. Equipment size and complexity: Electrodeposition requires specialized equipment, including plating baths, power supplies, and handling systems. Scaling up the manufacturing process would involve significant investments in larger equipment, increased maintenance, and more complex process control, making it less feasible for high-scale production.

4. Material limitations: Electrodeposition is primarily suitable for metals and some alloys. It may not be the ideal process for depositing other materials or complex structures, limiting its versatility for certain manufacturing applications [31, 32]

2.3.2.3. Plasma Activation

The method of oxygen plasma treatment, sometimes referred to as oxygen plasma etching or oxygen plasma cleaning, is employed in a number of sectors, including surface engineering, materials research, and semiconductor manufacturing. It includes modifying a material's surface properties by applying a low-pressure plasma that contains oxygen atoms, ions, and radicals [33]

Here's a general overview of how oxygen plasma treatment works:

Plasma generation: Using a radio-frequency (RF) power source, a low-pressure gas discharge is produced in a vacuum chamber. The process gas is commonly oxygen gas (O2).

Plasma activation: The oxygen gas is excited by RF power, resulting in the formation of oxygen atoms (O), ions (O+), and free radicals (O-) from the O2 molecules. This produces a plasma that contains oxygen species and is extremely reactive.

Surface interaction: The oxygen species in the plasma interact with the surface of the substance. The reactive oxygen atoms, ions, and radicals can etch some materials or chemically react with organic pollutants to remove surface oxides.

Surface Modification: Depending on the desired result, the plasma treatment might result in a variety of surface alterations. By eliminating organic residues, it can clean the surface. It can also increase the surface's wettability, improve adhesion, or alter the material's surface energy [34].

Treatment with oxygen plasma has various advantages, including:

Surface Cleaning: Organic pollutants, leftovers, and surface oxides can be successfully removed from a material by the reactive oxygen species in the plasma, leaving behind a clean surface.

Surface Activation: By forming functional groups on the material's surface, the plasma treatment can enhance the material's adhesion capabilities and foster bonding with other substances or coatings.

Etching: Oxygen plasma can occasionally be used as an etchant to remove specific materials with precision. The desired etch rate and selectivity are achieved by adjusting the plasma chemistry and process parameters.

 Surface Energy Modification: Depending on the needs of the application, oxygen plasma treatment can change a material's surface energy, making it more hydrophilic (attractive to water) or hydrophobic (repellent to water).

It's significant to note that depending on the material being treated, the plasma characteristics, and the desired result, the specific effects of oxygen plasma treatment can change. To obtain the intended surface modification or cleaning results, careful process optimisation must take into account the material attributes.

For this research, we are utilizing plasma activation to enhance NiO's interaction with the surface of FTO to improve the layer bonding and quality.

2.4. Material Characteristics

HTMs have specific properties that can be altered to enhance the effects it has on the devices. This modification is essential for novel research as basic inorganic materials used for ETMs have already been extensively studied. However, the basic, extremely used and studied HTM is Nickel Oxide (NiO). This section discusses the basics and types of NiO structures along with the state-of-the-art improvements brought by HTMs[35].

2.4.1. Nickel Oxide(NiO)

NiO shows high stability and performance. It is a p-type transition metal oxide. It is inserted between photoanode and the active layer and promotes hole extraction and their selective transport to the photoanode. It also behaves as an energy barrier to inhibit the transfer of electrons to the phtoanode. NiO possesses high work function and high transparency. NiO offers promising attributes as the HTL in OSCs due to its p-type character, wide bandgap (3.6–4 eV), high work function (5 to 5.6 eV), and admirable chemical stability. [36]

Similar to NaCl, NiOx has a cubic structure with a lattice parameter of 0.4173 nm. The structure is depicted in Fig 2.9 and can also be thought of as an octahedral one, with Ni2+ surrounded by O_2 at its centre. Because of NiOx's intrinsically strong ionisation energy and robust crystal structure, NiOx-based PSCs exhibit great photostability and thermal stability. Stoichiometric NiO typically has inherent conductivity below 10-4 S cm^{-1}, making it an insulator. However, too much oxygen causes nickel vacancies and holes, and while NiOx is being employed, it often displays properties of a p-type semiconductor. [37]
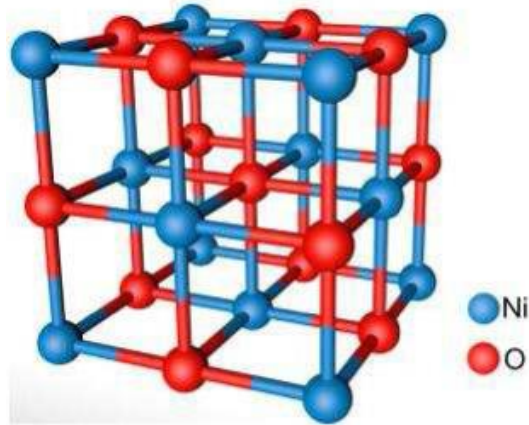
Figure 2. 9. Crystal structure of NiO

The optical transition of metal oxides, generally, depends on a number of internal energy states, primarily on the near-band edge (NBE) between the conduction band (CB) and valence band (VB). Other transitions in p-type metal oxide semiconductors are energy states brought about by intraband defects such metal deficit or excess oxygen. Due to Ni vacancy or interstitial oxygen, the NiOx film has a decreased band gap when formed at the greatest oxygen flow ratio [37] . Above the top of VB, in the energy states of Ni vacancy and Ni3+ in NiOx, which can accept electrons from VB as a p-type doping. [38]

To improve the adherence of film with the substrate, it is given oxygen plasma treatment. Better adherence is said to improve the device properties including FF(fill factor), short circuit current density (Jsc), transmittance, contact angle etc.[39]

Chapter 3.

Materials and Methods

3.1. Materials

Nickel acetate tetrehydrate, ethanol and acetic acid were purchased from Sigma-Aldrich. All these chemicals were of analytical grade and used without further purification. The fluorine-doped tin oxide (FTO) glass were used as substrates.

3.2. Synthesis of NiO sol

For the synthesis of NiO sol, Nickel acetate tetrahydrate works as the main precursor and acetic acid works as a stabilizer as it prevents cluster formation (aggregation process). Ethanol was used as solvent. Nickel acetate tetrahydrate(5mmol) was dissolved in ethanol(0.172mol). Both were added in a beaker and then stirred for 25min. After stirring the solution sonicated for 1.5 hr at 50°C. 3ml acetic acid was then added through pipette. The addition of acetic acid turned turbid solution into a clear one [40]
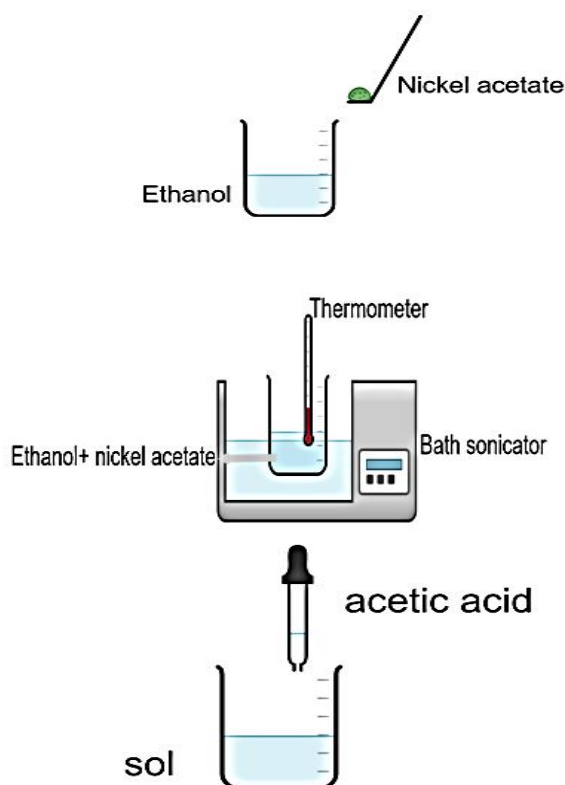
Figure 3. 1. Synthesis of NiO NPs

Thin film was prepared by three different methods, including:

1. Dip coating
2. Spin coating
3. Electrochemical coating

3.3. Thin Film formation by dip coating

To prepare NiO thin films from the synthesized sol, dip coating technique was used. This technique was selected depending upon the required thickness of thin film for specified application as well as its ease in large scale manufacturing.

Primarily, the substrates were carefully washed and cleaned in an organized manner to remove any organic impurities. This is important due to the dependency of thin film uniformity on the thickness and impurity free substrates especially for the thin films with thickness in nanometer ranges. Here, the FTO coated glass substrates were placed in distilled water and bath sonicated for 15-20 minutes followed by bath sonication in ethanol and in acetone for 15 minutes. Then the substrates were taken out of the beaker and placed in a drying oven at 60 °C for 15 minutes. [41]

After cleaning and drying, 3 FTO coated glasses were treated with plasma oxidation for 30min and 3 were left untreated. [41]

Next, the dried samples were placed in the sample holder of dip coater. The dip coater was set at a speed of 1416µm/sec. Firstly, the plasma oxidized FTO's were immersed each for 0min, 2min and 4min. Afterwards, un-oxidized FTO's were immersed each for 0min, 2 min and 4min. This resulted in thin layer formation on the slides. These slides were then placed on a hot plate maintained at 120ºC. The thin films formed onto slides were amorphous in nature and need annealing at higher temperatures to form poly-crystalline phases.

Figure 3. 2. Dip coating setup for making thin films.

The amorphous coated films are then placed in muffle furnace where 400ºC of temperature is achieved with an increment of 2^0C/min. The thin films then became polycrystalline and were nearly transparent. Uniformity varied with respect to plasma oxidation and time of immersion.[42]

3.4. Thin film formation by spin coating on FTO glass

To prepare NiO films through spin coating, 20µl of prepared solution was first dropped onto the middle of the substrate. This was done for 20s at 2000rpm. A layer of NiO was obtained. The slide was then kept at 120°C for 20min to remove ethanol. Further, it was placed in furnace at 400°C for 3hr20min. [43]

Glass slide

Spin coater

Dropping solution on slide

Coated glass

Glass slide

Heating plate

Annealing at 400°C
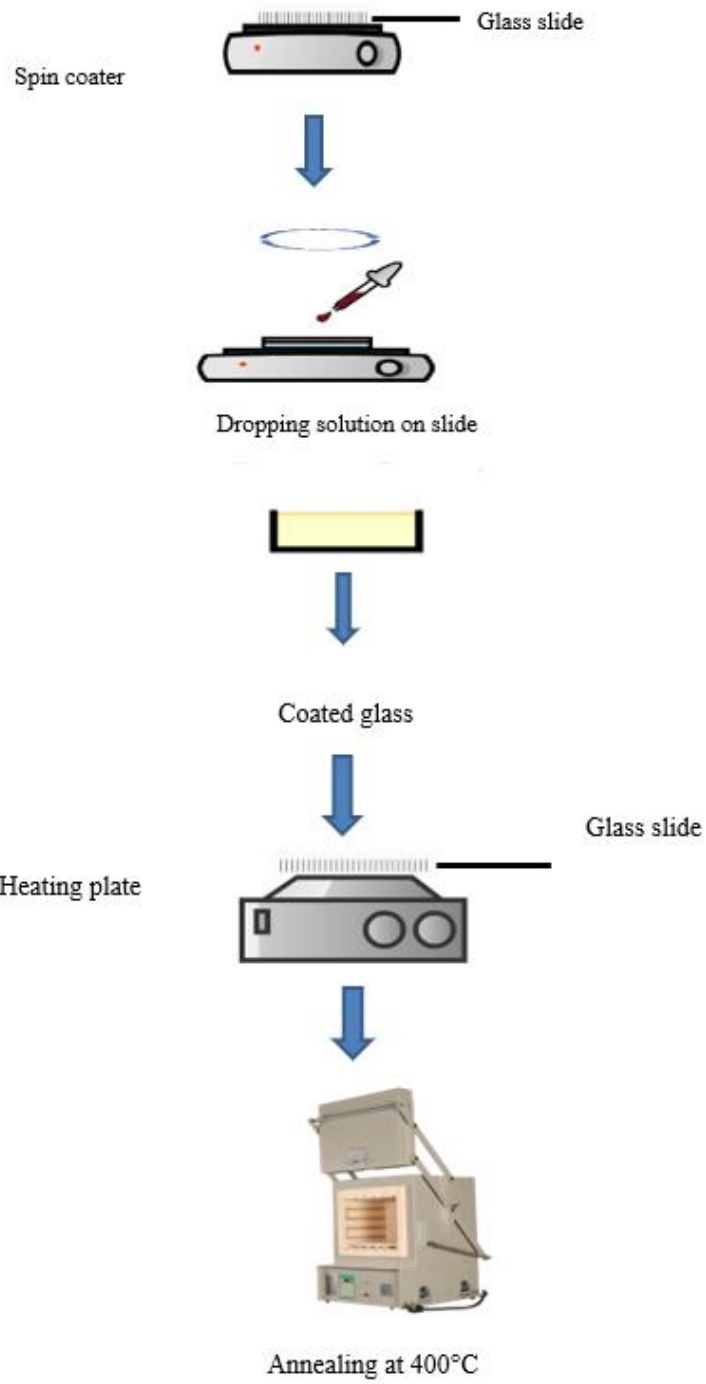
Figure 3. 3. Spin coating of NiO on FTO substrate via spin coating

3.5 Thin film preparation by electrodeposition on FTO glass

NiO thin film was prepared by electrodeposition via using a potentiostat. Ag/AgCl and Pt were used as reference and working electrode. 1M KOH was prepared to be used as an electrolyte in 50ml DI water and 0.1 M Ni $(NO_3)_2.6H2O$ was added to it. This three-electrode placement was done and a constant voltage of -1V was applied for 2 minutes. The deposited film was heated at 120°C for 20min. It was further annealed at 400°C for 3hr20min [44].
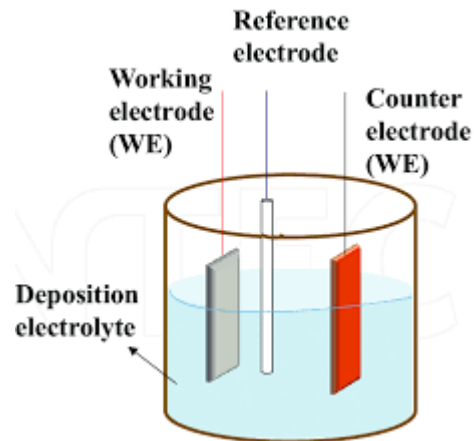
Figure 3. 4. Electrodepostion of NiO on FTO substrate

Chapter 4

Characterization techniques

4.1. Instrumentation and measurements

The morphological properties of the samples were examined using a scanning electron microscope (SEM) from Tokyo, Japan, equipped with an EDS . The structural characteristics were analyzed using X-ray diffraction (XRD) on a Seimens D5005 STOE & Cie GmbH instrument from Darmstadt, Germany, with data collected in the angle range of 10° to 80° (2θ). Fourier-transform infrared (FTIR) analysis was performed on a PerkinElmer SpectrumTM100 spectrophotometer using potassium bromide pellets to analyze the dried powder samples. Raman spectra were obtained using a BWS415-532S-iRaman device manufactured by BW TEK INC from Newark, NJ, USA. UV-Vis spectrum measurements were performed.

4.2. Scanning Electron Microscopy (SEM)

The most widely used technique for high-resolution imaging of materials is the scanning electron microscope (SEM). This powerful tool magnifies the features of a material, making it possible to visualize details that are not visible to the naked eye. SEM achieves this by using a beam of high-energy electrons to scan the surface of the object. [45]

The electron beam in SEM has a much smaller wavelength, enabling it to reveal even minute details. Its resolution can be up to one million times greater than the original size of the object, making it invaluable for researchers working at micro and nano levels. SEM's resolution is approximately 1000 times better than that of the human eye, which has a resolution of about 200 µm (0.2 µm).

The superior resolution of SEM, compared to a light microscope, is due to its utilization of a beam of electrons accelerated with a voltage of 100kV. SEM can analyze both conductive and non-conductive materials. When coupled with an Energy-Dispersive X-ray Spectroscopy (EDS) detector, it can provide elemental analysis of the sample, offering both qualitative and quantitative information about the material's composition. [46]

To conduct SEM imaging, samples are placed on a stub inside the sample chamber and are usually coated with a thin layer of gold to improve imaging quality. The upper cathode assembly, also known as the electron gun, is connected to a high-voltage

power cable (ranging from 30kV to 40kV) and generates electrons that are accelerated down the chamber.

There are four types of electron guns commonly used in SEM: Schottky field emission, cold field emission gun, LaB6 emitter, and tungsten filament, with tungsten being a common choice. After electron generation, an electron energy spread occurs, where most electrons have an energy close to the accelerating voltage (e.g., 20 keV for a 20 kV operating voltage). Electron lenses at different planes capture electrons with varying velocities, with low energy spread electrons being easier to capture and producing clearer images.

The beam is focused into a probe by electromagnetic lenses, which then scans the area of the material in a raster pattern. This probe is then reconverged by the condenser lens, creating a fine probe through the objective lens. The backscattered electrons and secondary electrons emitted from the sample are detected by backscattered and secondary detectors, respectively. The entire setup operates under vacuum conditions. The detected signals create an image displayed on the screen, which results from the interaction between the emitted signals and the sample. These signals are amplified and processed to provide detailed and informative SEM images. [47]
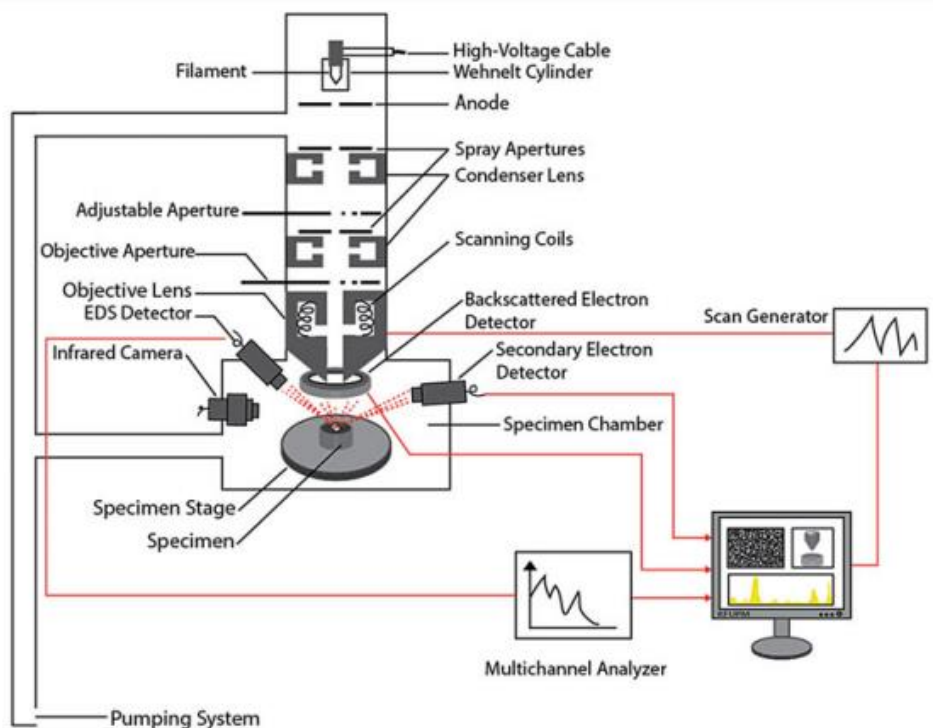
Figure 4. 1. Schematic construction and working of SEM [48]

4.3. X-ray Diffraction (XRD)

The X-ray diffraction (XRD) technique is a crucial method used to characterize material, based on the interaction of X-rays with the sample. By analyzing the reflections of X-rays, valuable information about the crystalline structure, grain size, microstructure, and average particle size of the material can be obtained.

XRD works on the principle of Bragg's law, which relates the diffraction angle (θhkl) of a specific hkl reflection and the spacing of planes (d_hkl) in the crystal lattice to the wavelength (λ) of the incident X-rays:

$$2dhkl \times sin\theta hkl = \lambda$$

This non-destructive technique provides a unique fingerprint of Bragg's reflections in a reciprocal space, allowing for detailed analysis of the crystal structure.

To generate X-rays, a metal surface, typically copper (Cu), is bombarded with electrons, resulting in the scattering of these electrons by the cloud of electrons surrounding each atom in the sample. When these scattered X-rays strike the sample's surface, a phenomena of constructive interference occurs, and the path difference (λ) is equivalent to 2d sin θ is observed. The angle 2θ is experimentally measured as the detector or sample is moved.

The crystal acts as a three-dimensional diffraction grating, producing diffraction spots in a reciprocal lattice when the X-ray beam interacts with it. These diffraction spots are inversely related to the crystal planes and the dimension of the crystallites present in the material. The crystal planes are associated with real space and diffraction spots are related to reciprocal space, and together they create a three-dimensional reciprocal lattice, providing valuable information about the material's crystal structure and characteristics. [49]
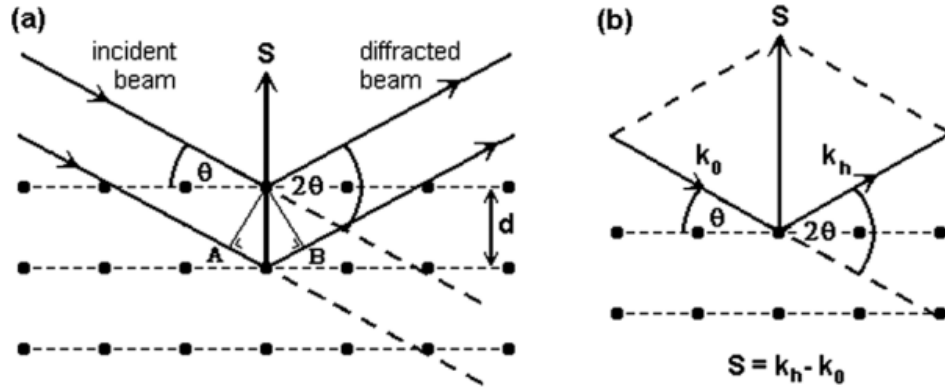
Figure 4. 2. Diagram of x-ray diffraction; (a)representation of the conditions required for Bragg diffraction to occur and (b) relationship of the incident (k0), diffracted (kh) and scattering (S) vectors with respect to the crystal

4.4. UV-Visible Spectrometer

The described technique involves measuring the absorption of light as a function of wavelength to gather information about the transitions of electrons within a material. It specifically helps determine the band gap, which refers to the difference of energy between the conductance and valence electron shells. The method is based on the Bohr-Einstein equation, which relates the energy difference (ΔE) between two states (E2 and E) to the frequency (ν) of electromagnetic radiation:

$$\Delta E = E2 - E = h\nu$$

Here, h is Planck's constant, with a value of 6.626×10^{-34} Js. In optical spectroscopy, it is more common to use the wavenumber (ν) instead of frequency (ν), and the following equation is used:

$$\Delta E = E2 - E = hc\nu$$

In this equation, c represents the speed of light. By measuring the absorbed or emitted radiation of a specific frequency or wavelength, different energy differences can be identified.

Modern spectrophotometers typically incorporate both visible and UV sources, which are then split into their constituents using a prism or grating monochromator, a method known as the dispersive method. In a double-beam instrument, the light beam is split into two paths, with one directed toward a reference material and the other toward the sample. The light from both paths is then refocused and falls onto a detector, which

generates an alternating current (AC) signal. This signal is displayed in the form of a wave, providing valuable information about the sample's absorption characteristics.

For measurements, solid particles are usually dispersed in a solvent to create dispersions, while liquids are directly used with varying dilutions. Cuvettes are employed to hold the sample during measurement, and they are typically positioned around 10-15 cm apart.

Overall, this spectroscopic technique allows researchers to gain insights into the electronic transitions and band gap of materials, aiding in the study of their optical properties and behaviors. [50]
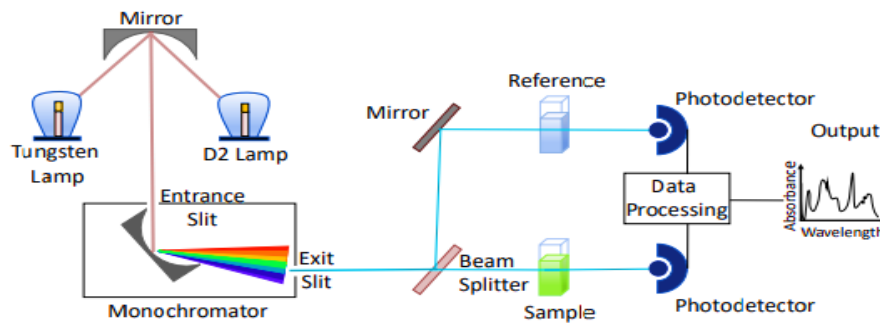
Figure 4. 3. Schematic showing the working of a double beam UV vis spectrophotometer

4.5. Profilometry

Profilometry is a non-destructive measurement method widely employed to determine the thickness of thin films on a substrate. It is a vital tool in materials science, semiconductor manufacturing, and diverse thin-film applications, providing crucial insights into the film's surface topography and step heights.

At its core, profilometry involves running a sharp stylus or probe along the film's surface and recording the vertical displacement of the probe during the scan. This displacement data is then utilized to generate a surface profile, which unveils height variations related to changes in the film's thickness.

A profilometer includes a stylus or probe mounted on a measurement head, allowing vertical and lateral movement across the sample surface. The stylus usually has a sharp tip for high spatial resolution. Before measurements, the profilometer is calibrated using a standard reference sample with known dimensions to establish the relationship between probe displacement and corresponding height changes. The thin film under examination is deposited on a substrate with known thickness and properties. The substrate serves as a reference point, and its thickness is subtracted from the total

measured thickness. The measurement head scans across the sample surface, and the probe gently touches the film. The probe's vertical movement records the surface topography, and this data is correlated with the lateral position. The instrument records the displacement data, enabling the creation of a surface profile that displays height variations (film thickness) across the sample. The profilometry data is further analyzed to calculate film thickness at specific points or defined regions of interest. Statistical analysis provides average thickness and uniformity information. The film thickness is determined by measuring the difference between the highest and lowest points in the surface profile, which corresponds to the step height and relates to the film thickness. Profilometry provides valuable information about film's thickness, roughness and uniformity[51].
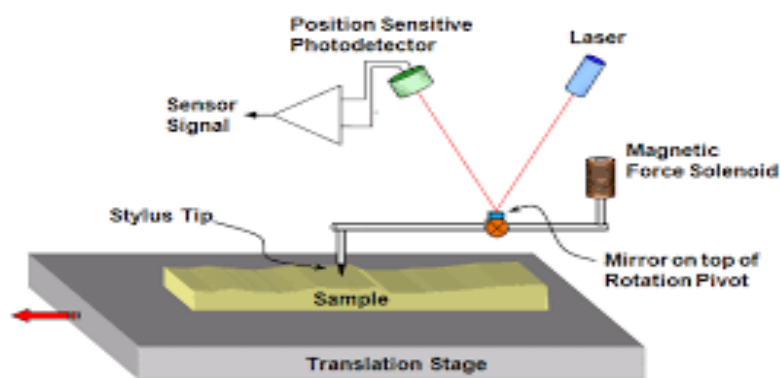
Figure 1 Basic elements of a stylus profilometer.

Figure 4. 4. Schematic showing working of a profilometer

4.6. Cyclic Voltammetry (CV)

Oxidation-reduction (redox) reactions are fundamental electrochemical processes that involve the exchange of electrons between species. Cyclic voltammetry is an electrochemical technique extensively used to investigate these redox reactions and study the electrochemical behavior of a system. It provides valuable information about the redox potentials, kinetics, and reversibility of reactions.

In cyclic voltammetry, the redox reactions take place at the working electrode, which is the surface under examination. The technique involves applying a controlled

potential to the working electrode while simultaneously measuring the current flowing through it.

The experiment is performed in an electrochemical cell containing three primary components: a working electrode (often a conductive material or an electrode coated with the substance of interest), a counter electrode (typically made of inert material like platinum), and a reference electrode (used to measure the potential difference).

experiment commences with a potential scan. The potential of the working electrode is varied linearly with time over a defined range. The scan usually starts from a negative value (cathodic region) and progresses to a positive value (anodic region).

As the potential of the working electrode is changed, redox reactions occur at its surface. During the cathodic sweep (negative potential), reduction reactions take place, where species gain electrons and become reduced. Conversely, during the anodic sweep (positive potential), oxidation reactions occur, leading to the loss of electrons and the oxidation of the species.

The current flowing through the working electrode is simultaneously measured during the potential scan. The measured current provides information about the rate of the redox reactions taking place at the electrode surface.

After the potential scan reaches its maximum value, it is reversed, and the scan returns to the negative potential region. This reverse sweep allows the system to undergo the reverse redox reactions.

The potential sweep is repeatedly cycled back and forth between the cathodic and anodic regions. Each cycle enables the observation of the redox reactions in both directions, providing information about the reversibility of the electrochemical reactions.

The resulting cyclic voltammogram, a plot of current versus potential, is analyzed to determine the redox potentials, peak current values, and other electrochemical parameters. The shape of the cyclic voltammogram offers insights into the reversibility and kinetics of the redox reactions.

Cyclic voltammetry is a reliable tool in electrochemistry, widely used in various fields, including analytical chemistry, materials science and the study of electrochemical processes in biological systems. It enables researchers to gain a deeper understanding of redox reactions and the behavior of electroactive species, making it a valuable technique for characterizing electrochemical systems. [52]
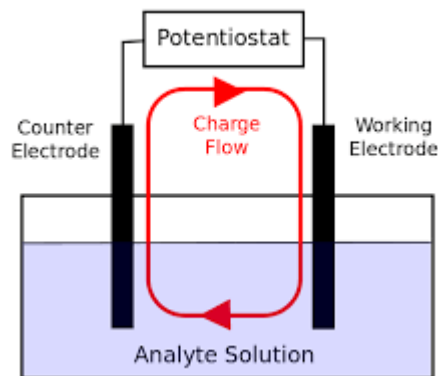
Figure 4. 5. Schematic showing working of CV

4.7. Electrical impedance spectroscopy (EIS)

Electrical impedance spectroscopy (EIS) is a highly effective method used to investigate the electrical characteristics of materials and systems across a broad range of frequencies. It provides valuable insights into impedance, encompassing resistance and reactance, of diverse samples, including materials, biological tissues, electrochemical systems, and electronic components.

The underlying principle of EIS involves applying an alternating current (AC) signal with a known frequency to the sample and then measuring the resulting voltage response. This AC signal is typically sinusoidal, and the frequency is varied over a wide spectrum, spanning from very low frequencies (millihertz) to high frequencies (gigahertz).

An electrical impedance spectrometer is utilized, consisting of a signal generator responsible for producing the AC signal with adjustable frequency and amplitude. A sensitive voltmeter or impedance analyzer is employed to measure the voltage response of the sample. The sample is prepared according to the specific application. For instance, in the case of biological tissues, the sample may be in the form of cell suspensions or tissue slices, while in electrochemical systems, it could involve an electrode immersed in an electrolyte. The AC signal is applied to the sample, and the system records the amplitude and phase of the voltage response concerning the input signal. The frequency of the AC signal is systematically varied, and the impedance response is recorded at each frequency point. The frequency sweep is conducted over a wide range to gain a comprehensive understanding of the material's electrical behavior. The measured impedance response is analyzed to extract valuable information. Plotting the impedance as a function of frequency generates an

impedance spectrum or Nyquist plot, often represented as a semicircular arc. This plot provides valuable insights into different aspects of the sample's electrical properties. The acquired impedance spectrum can be further examined using mathematical models or equivalent circuit elements to comprehend the underlying physical processes contributing to the impedance response. Model fitting facilitates the extraction of specific electrical parameters, such as resistances, capacitances, and inductances.

Electrical impedance spectroscopy finds wide applications in fields like material science, bioengineering, electrochemistry, and electronics. It is commonly employed to study the electrical properties of batteries, fuel cells, sensors, biological tissues, as well as to assess the performance of electronic components and materials. EIS's capability to provide information across a broad frequency range makes it an invaluable tool for understanding the electrical behavior of complex systems and materials.[53]
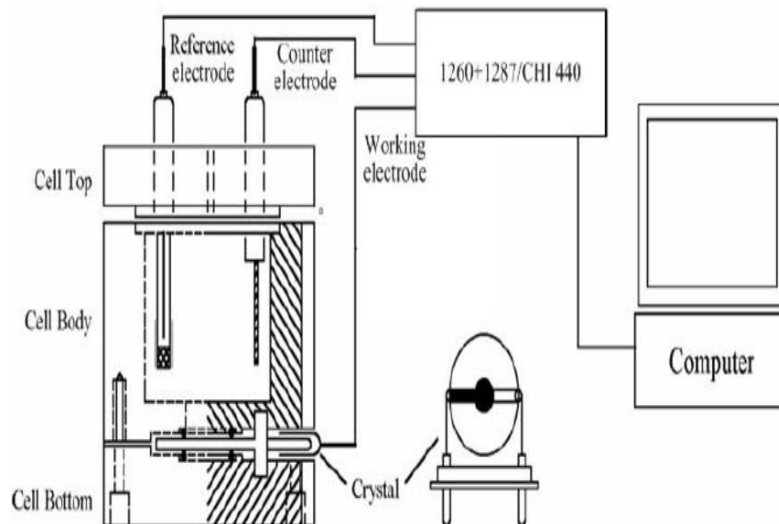
Figure 4. 6. Schematic showing working of EIS[54]

4.8. Hall effect measurement

Hall effect measurement is a widely utilized technique to determine the electrical conductivity and carrier concentration of thin films. It relies on the Hall effect, which causes an electric field to develop perpendicular to both the direction of an electric current and an applied magnetic field in a conductive material. The thin film sample is carefully fabricated or deposited onto a suitable substrate. The film needs to possess sufficient conductivity to enable Hall effect measurements.

The measurement setup consists of a sample holder that secures the thin film sample and electrical contacts. Typically, four electrical contacts are employed for Hall effect measurements: two for passing the current through the sample (current contacts) and two for measuring the voltage across the sample (voltage contacts). A known electric current is applied through the current contacts, while a perpendicular magnetic field is applied to the thin film surface. The magnetic field is usually generated using either a permanent magnet or an electromagnet.

As the current flows through the thin film in the presence of the magnetic field, the Hall effect causes an accumulation of charge carriers on one side of the film. This accumulation generates a voltage across the film's thickness, perpendicular to both the current and the magnetic field. This voltage is referred to as the Hall voltage (VH).

 The Hall voltage (VH) is measured using the voltage contacts, and the magnetic field strength (B) is known. Using these values, the carrier concentration (n) and electrical conductivity (σ) of the thin film can be calculated using the following equations:

- Carrier concentration (n) = 1 / (e * RH * B) Here, e represents the elementary charge, and RH is the Hall coefficient, which can be obtained from the slope of the VH vs. magnetic field plot.

- Electrical conductivity (σ) = (I * d) / (VH * B) In this equation, I represents the current, d is the thickness of the thin film, and VH is the Hall voltage.

Hall effect measurements on thin films provide valuable insights into their electrical properties, such as the type of charge carriers (electrons or holes), their concentration, and the level of electrical conductivity. This information is crucial for understanding the behavior and performance of thin films in various electronic and optoelectronic applications. [55]
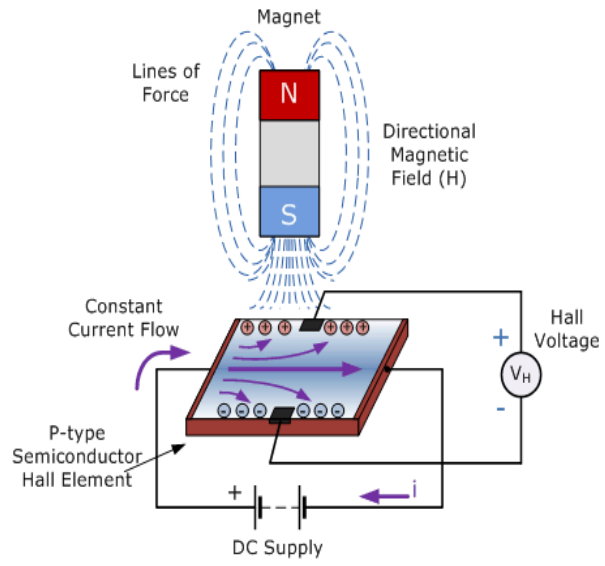
Figure 4. 7. Schematic showing working of Hall effect instrumentation.[56]

Chapter 5

Results and Discussion

5.1. Scanning Electron Microscopy (SEM)

The results in figure 5.1 show the SEM results for NiO coated through electrodeposition (5.1a) and spin coating (5.1b). Both the samples were plasma treated before coating with NiO. These two processes do not show good surface coverage however the sample prepared through spin coating shows comparatively better results than the one prepared by electrodeposition. This is because electrodeposition has tendency towards non conformal growth on non planar surfaces. This is because the electrons gather in asperities of these surfaces. Due to this, more deposition occurs at these points which only makes the surface rougher. Additives in the plating bath can also create this issue by gathering at the points of highest current density and thus inhibit deposition.

Spin coating showed better results than electrodeposition but still film quality was not as expected. This is because this process applies liquid coating on solid substrate which is then spun at a controlled speed. Centrifugal forces come into play due to rapid spinning and a lot of coating material is lost during spinning. This results in the formation of non-uniform coatings.
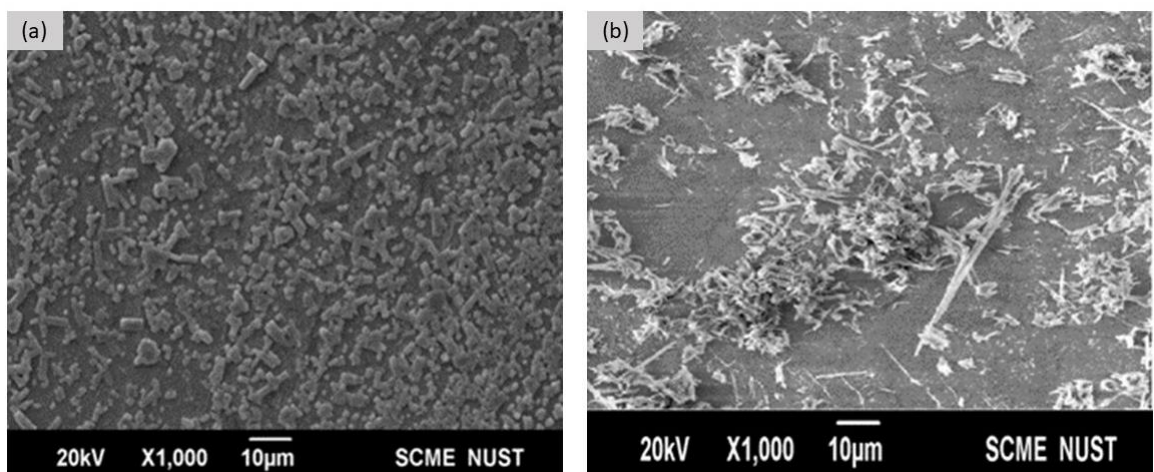
Figure 5. 1. SEM Images (a) NiO coating through electrodeposition (b) NiO coating through spin coating

6 samples were prepared through dip coating. 3 FTO's were coated with NiO through dip coating at 0min, 2min and 4min coating time. **Figure 5.2 (a) to (c).** The remaining 3 FTO's were first subjected to plasma treated for 30min and then dip coated for 0min, 2min and 4min respectively. **Figure 5.3 (a) to (b).** The samples prepared after plasma activation showed better adherence and uniform coating.
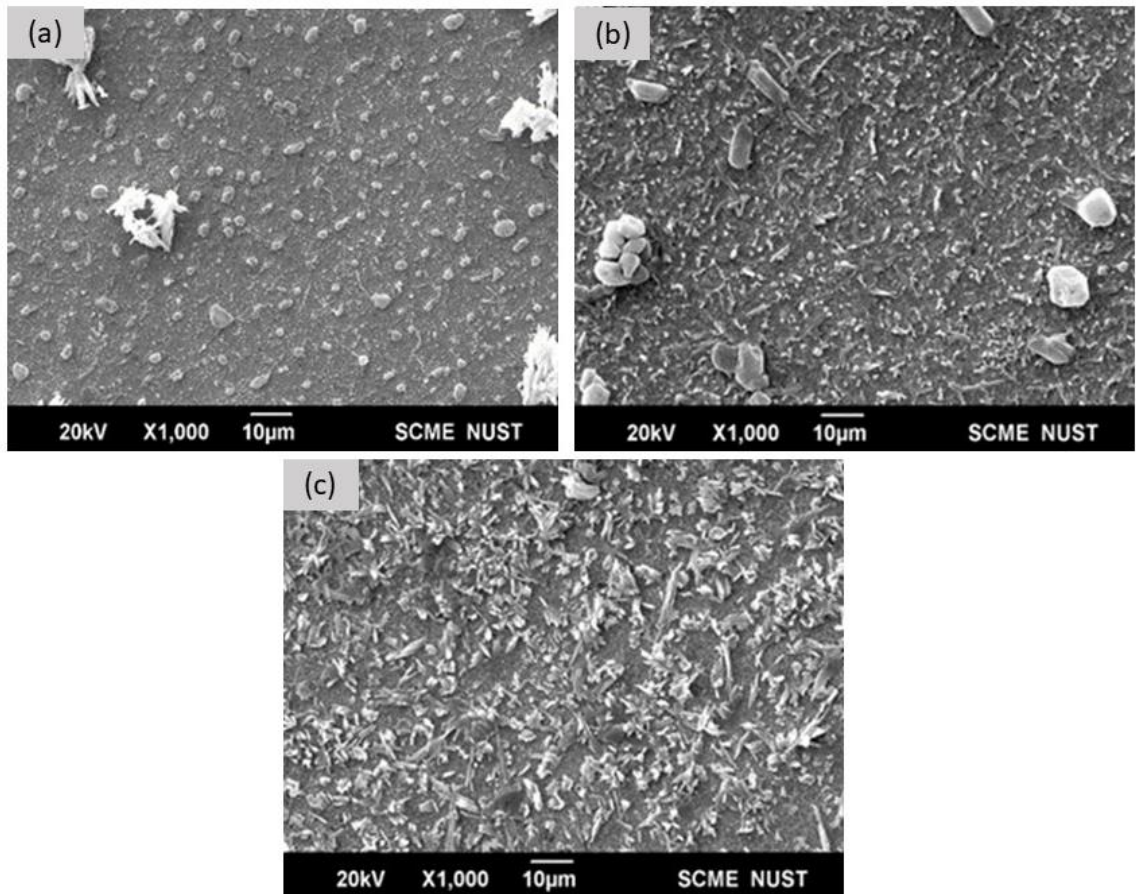
Figure 5. 2. SEM Images of without activation (a) NiO coated for 0 min (b) NiO coated for 2min(c) NiO coated for 4min dipping time
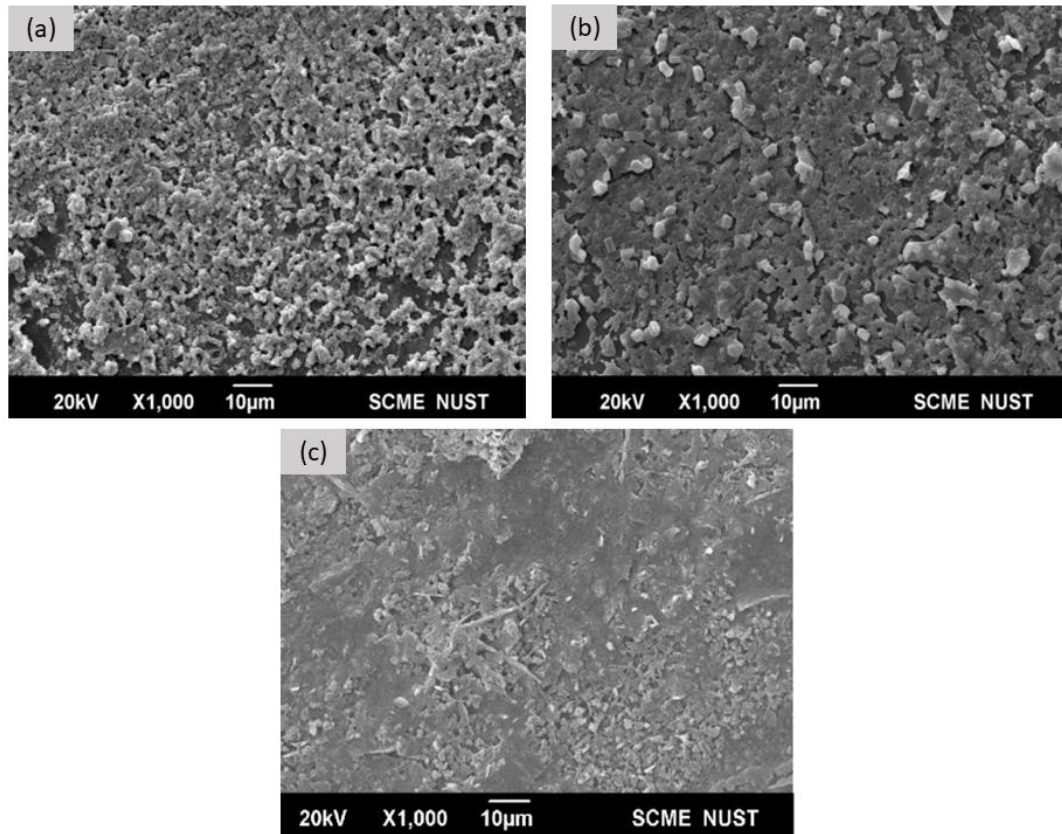
Figure 5. 3. SEM Images of with plasma activation (d) NiO coated for Omin (e) NiO coated for 2min (f) NiO coated for 4min dipping time

5.2. Energy Dispersive X-ray spectroscopy

The NiO thin film, synthesized through a dip coating, underwent elemental composition analysis using energy-dispersive X-ray spectroscopy (EDS). Figure 5.4. illustrates the EDS spectrum, providing conclusive evidence of the presence of both Ni and O elements in the prepared films. The presence of F and Sn is because of the FTO used as substrate material.

Figure 5. 4. EDS of NiO thin films

5.3. X-ray Diffraction (XRD)

X-ray results of bare FTO, NiO powder, NiO thin film deposited through dip coating, spin coating and electrochemical deposition are displayed in figure 5.4.

Figure 5.5a shows the XRD pattern of bare FTO. The appeared peaks in the XRD pattern are compared with the standard card (JCPDS 41-1445) for the FTO substrate. The Miller indices of FTO are (110), (101), (211), (220) (310), (301) corresponding to 30.615°, 33.822°, 51.63°, 54.420°,61.721° and 65.579°.

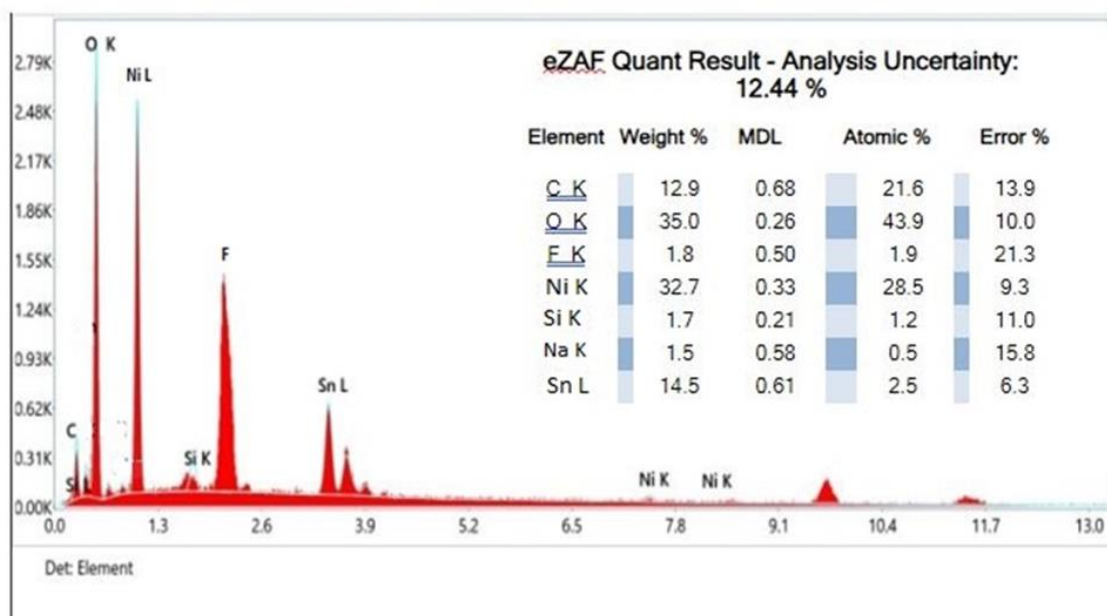 The XRD analysis of NiO powder Figure 5.5 b reveals distinct diffraction peaks at 2θ angles of 37.009°, 43.165°, and 62.672°, which can be confidently identified as corresponding to the (1 1 1), (2 0 0), and (2 2 0) crystal planes of bulk NiO, respectively. These diffraction peaks not only match perfectly in their positions but also exhibit relative intensities consistent with the standard spectrum (JCPDS, No. 02-1216) for cubic-structured NiO [57]. Additionally, the XRD pattern confirms that the samples are composed solely of the cubic phase of NiO, as no impurities or distinct diffraction peaks were detected, ensuring a single-phase sample. This result indicates that the physical phases of the NiO have higher purity prepared in this work.

Dip coated NiO on FTO is shown in Figure 5.5c. It shows a few peaks corresponding to FTO and all major peaks of NiO are observed. A slight peak shift in peak corresponding to miller index (220) is observed.

Spin coated NiO on FTO is shown in Figure 5.5d. It shows a few peaks corresponding to FTO. The NiO peak at miller index (111) is observed with the same intensity however, peaks at miller indices (200) and (220) show decreased intensity.

Electrodeposited NiO on FTO is shown in Figure 5.6e. A few peaks of FTO substrate are observed. The peak at miller index (111) corresponding to NiO is not observed. This is due to the non-uniformity of NiO layer.
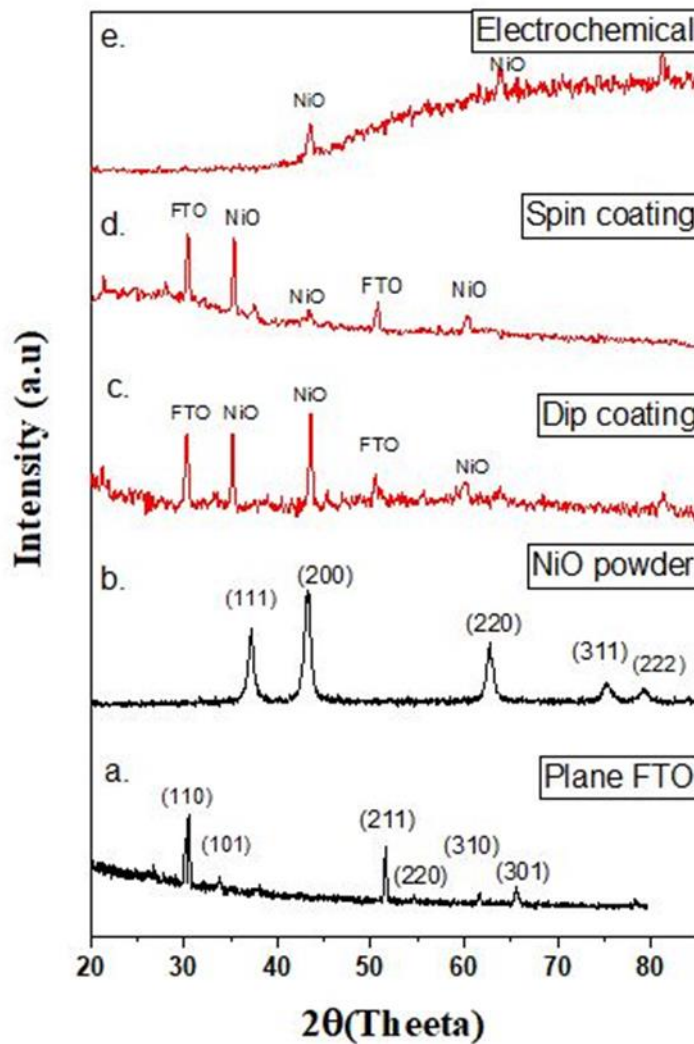

Figure 5. 5. (a) XRD of bare FTO (b) NiO powder (c) NiO layer through dip coating (d) NiO layer through spin coating (e) NiO layer through electrodeposition.

5.4. Raman spectroscopy

Raman spectrum of dip coated NiO thin films is shown, which exhibits five distinct peaks. Among them, the prominent peaks at approximately 557 and 1095 cm−1 correspond to the first-order longitudinal (LO) mode and second-order longitudinal (2LO) mode of NiO, respectively. These peaks are associated with the vibration of Ni-O bonds. Notably, the sharp peak at around 557 cm−1 indicates the presence of Ni defects. Additionally, the peaks observed at 460 and 780 cm−1 correspond to the first-order transverse mode (TO) and second-order transverse mode (2TO), respectively [58].
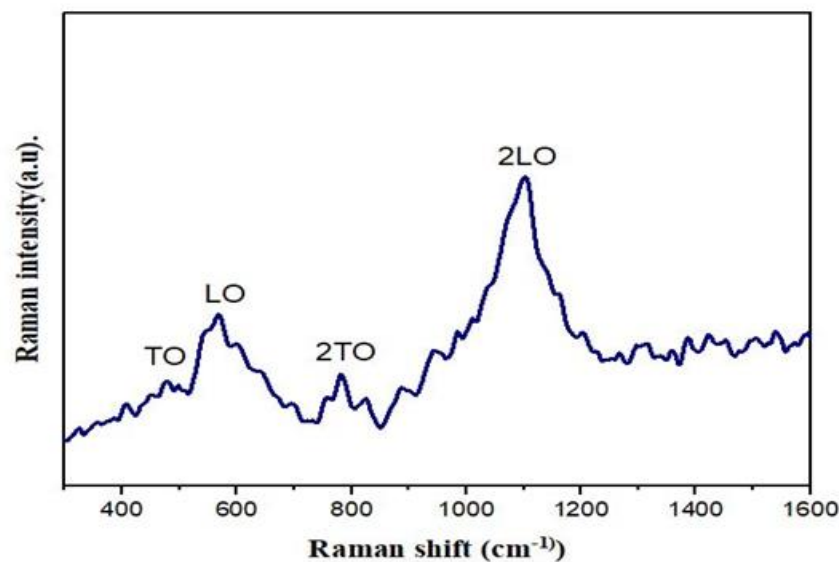
Figure 5. 6. Raman spectroscopy of NiO thinfilms

5.5. UV spectroscopy

All the samples were subjected to UV Vis treatment in a range of 250nm-600nm. The untreated samples showed comparatively lower transmittance as compared to plasma treated samples. The transmittance of untreated samples for 0min,2min and 4min dipping time was 30.7, 57.7 and 62.1 Figure5.7(a) which drastically increased to 59.5,70.3 and 72.5 respectively. Figure 5.7(b).
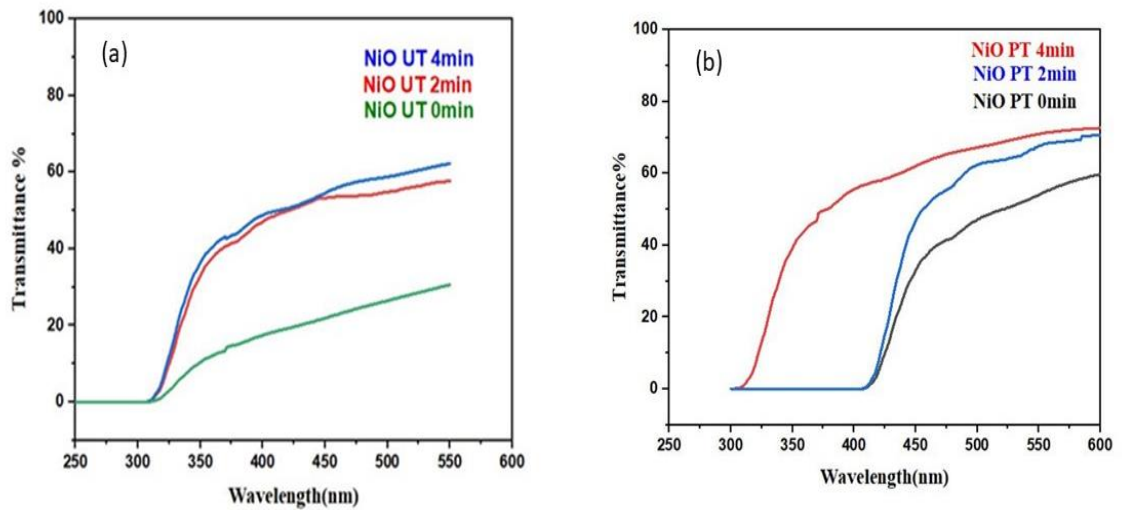
Figure 5. 7. (a) Transmittance of plasma untreated samples for dipping time 0, 2, 4 min (b) Transmittance of plasma treated samples for dipping time 0, 2, 4 min.

5.6. Band gap study

UV-Vis data can be utilized to find out the bandgap of each sample. E_g of samples for direct bandgap was calculated by using the formula, where n =2

$$ahv = A (hv-Eg)^n$$

The graphs are plotted amongst $(ahv)^2$ and E (eV), the first absorption curve is then extrapolated to the x-axis and that gives the value for the bandgap.

The band gap for untreated sample at 0min dipping time is the lowest which consequently increases as dipping time increases. Plasma treated samples have higher band gaps comparatively. The band gap trend observed for untreated samples is 3.62, 3.68 and 3.7 for 0, 2 and 4min dipping time. Figure 5.8 (a,b,c). After plasma treatment the bandgap observed is 3.73, 3.84 and 3.96 for 0, 2 and 4min dipping time respectively. Fig 5.8 (d,e,f)
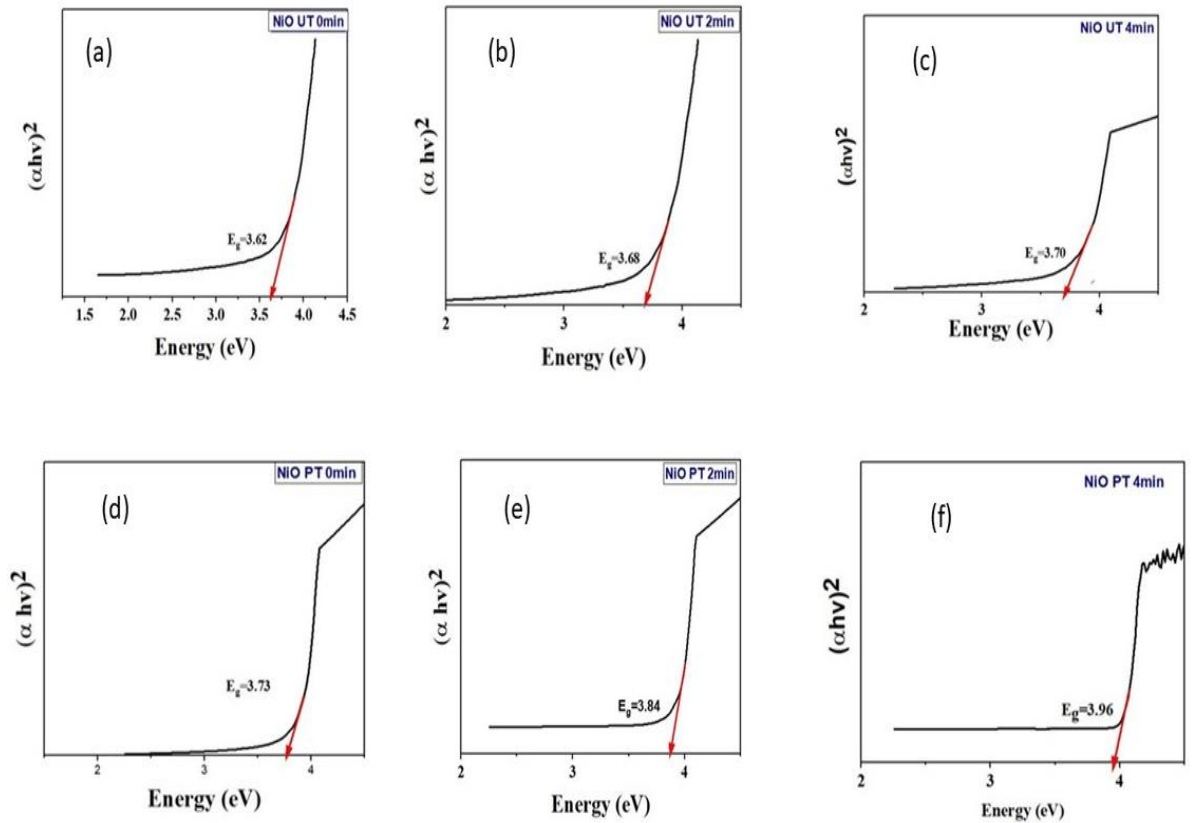
Figure 5. 8. (a) Eg for untreated sample at dipping time 0min.(b) Eg for untreated sample at dipping time 2min. (c) Eg for untreated sample at dipping time 4min. (d) Eg for plasma treated sample at dipping time 0min. (e) Eg for plasma treated sample at dipping time

5.7. Profilometry

After dipping the samples in the prepared NiO slurry for 0,2 and 4 minutes onto both untreated and treated FTO glass substrates, they were subjected to profilometry to find out the thickness of the films coated. The mean height of the untreated samples was 2.99 μm, 234 nm, 206 nm whereas for the treated samples the layer appeared to be rather thin as their mean heights were 149 nm, 115 nm and 108 nm. This can also be related to the transmittance that showed that for untreated samples the transmittance was low whereas for plasma treated samples, transmittance improved.
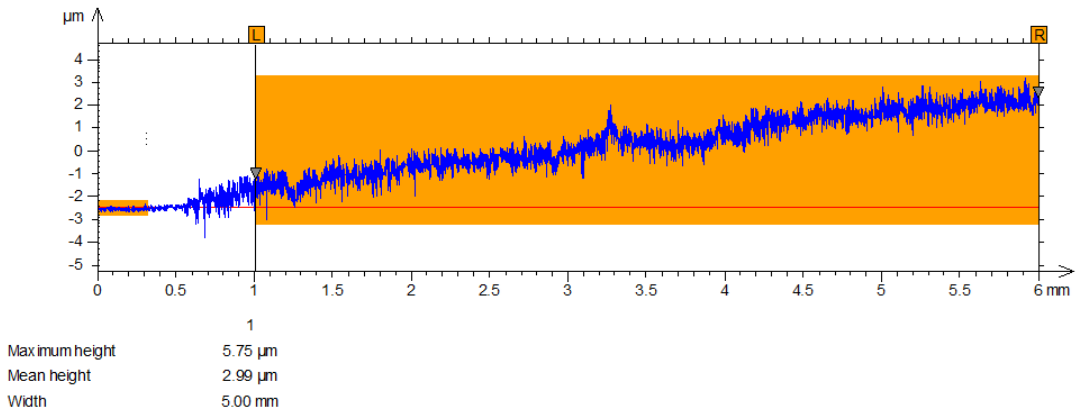
Figure 5. 9. Profilometry profile of untreated sample for 0 minutes
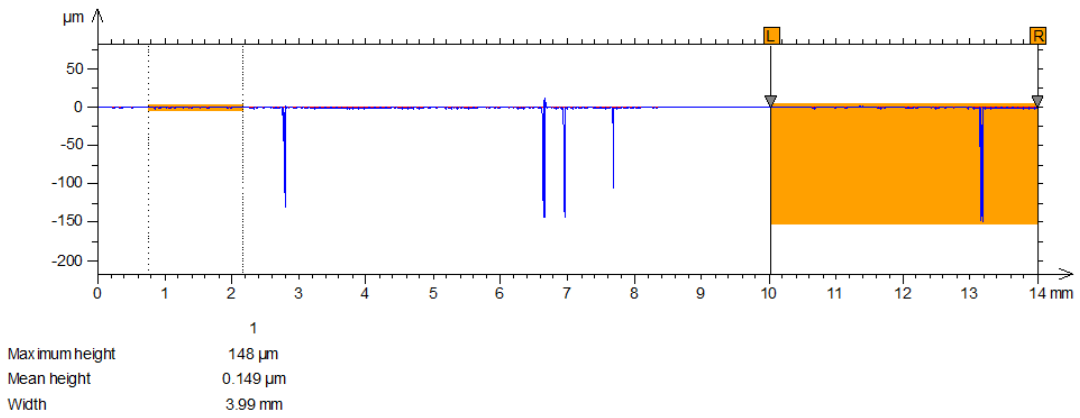
Figure 5. 10. Profilometry profile of untreated sample for dipping time 2minutes
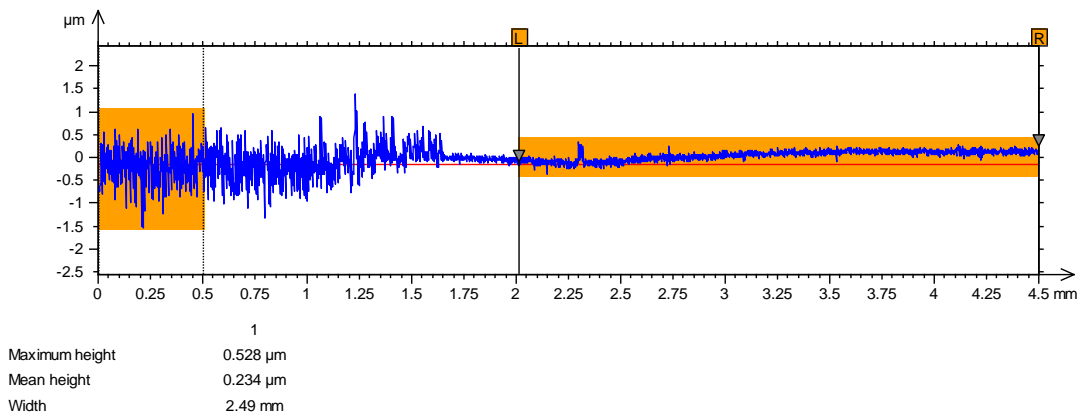
Figure 5. 11. Profilometry profile of untreated sample for dipping time 4 minutes
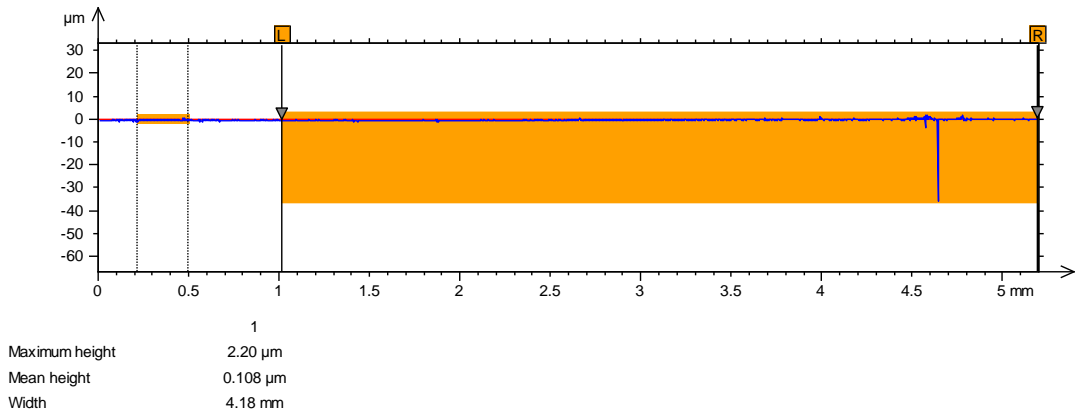
Figure 5. 12. Profilometry profile of treated sample for 0 minutes

Maximum height	2.20 µm
Mean height	0.108 µm
Width	4.18 mm
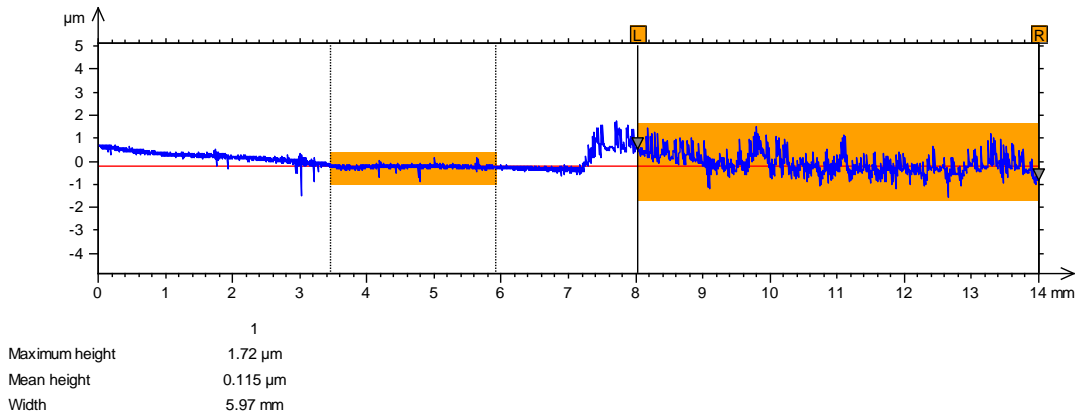
Figure 5. 13. Profilometry profile of treated sample for 2minutes

Maximum height	1.72 µm
Mean height	0.115 µm
Width	5.97 mm
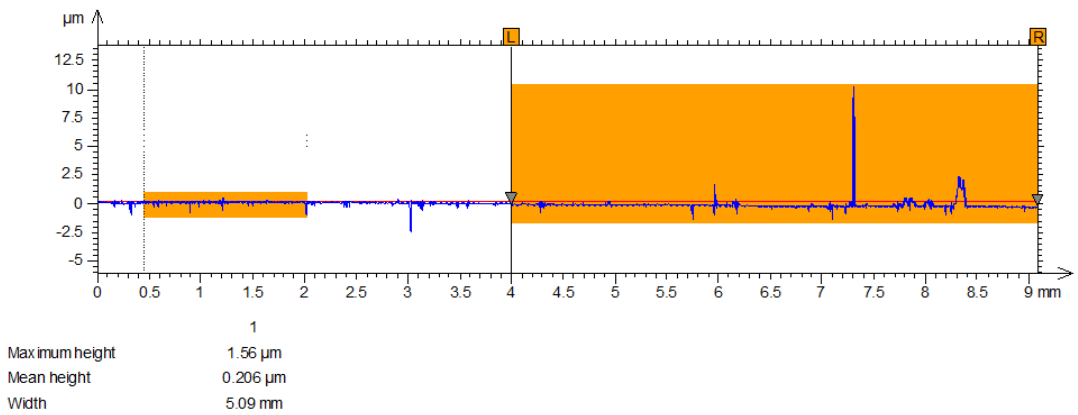
Figure 5. 14. Profilometry profile of treated sample for dipping time 4 minutes

Maximum height	1.56 µm
Mean height	0.206 µm
Width	5.09 mm

Table 1. Thickness Profile

Time	Untreated samples	Treated samples
0min	2.99 μ	108 nm
2 min	149 nm	115 nm
4min	234 nm	206 nm

Table 2. Roughness Profile

Time	Untreated samples	Treated samples
0min	300 nm	60 nm
2 min	50 nm	48 nm
4min	40 nm	36 nm

5.8. Cyclic Voltammetry

A three-electrode setup was used to perform cyclic voltammetry of films. The working electrode were the NiO deposited FTO samples, Ag/AgCl was used as a reference electrode and Pt wire was utilized as a counter electrode. All the readings were taken in 2M KOH solution. The scan rate of 100mV/s in a potential range of 0V - 0.5V was applied to carry out the measurements. [59]

The figure below shows the CV curves for the NiO samples made by dip coating for 0, 2 and 4 minutes onto the untreated FTO substrate. The samples showed significant reduction and oxidation peaks, the peak currents were recorded to observe the increasing trend of current. The peak current values were **0.12mA, 0.49mA, 0.51mA** at a potential of **0.390V, 0.398V, 0.401** for untreated samples dipped at **0, 2 and 4 minutes** respectively. The increase in the peak values indicate that the gaps observed in the uniformity of the NiO layer deposited in SEM images effect the transfer of charges across the film and therefore the sample that was dipped for 4 minutes

exhibited relatively uniform adherence of the thin film [60].Moreover, the conductive nature of FTO glass aided this flow of current.
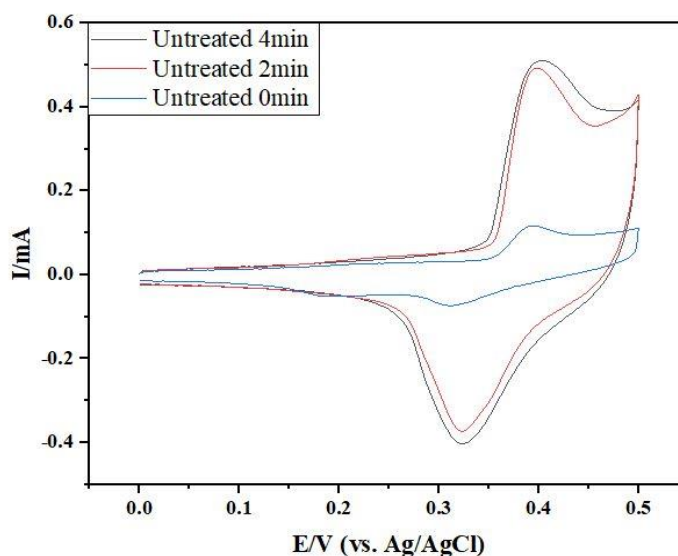
Figure 5. 15. CV curves of untreated FTO substrate dip coated samples.

The figure below shows the CV curves for the NiO samples made by dip coating for 0, 2 and 4 minutes onto the treated FTO substrate. The samples showed significant reduction and oxidation peaks, the peak currents were recorded to observe the increasing trend of current. The peak current values were **1.14mA, 1.18mA and 1.2mA** at a potential of **0.467V, 0.464V** and **0.462V for** the treated samples dipped at **0, 2 and 4 minutes** respectively. The SEM images for treated samples showed uniform films and making 4 minutes the best dipping time to achieve an optimum thin film that allowed maximum charge transfer.

The rise in anodic and cathodic current for untreated and treated samples was observed which indicates that the amount of positive and negative charge carriers incorporated into the film increases with time, signifying that the reaction activity of the NiO thin film improves with time and uniformity [61].
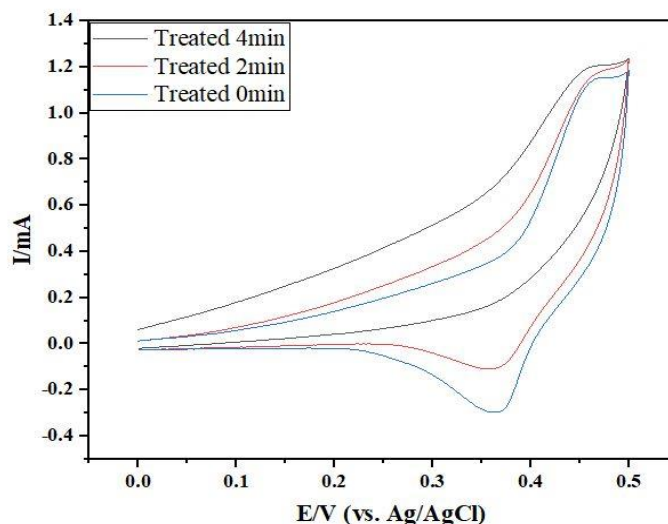
Figure 5. 16. CV curves of treated FTO substrate dip coated samples.

5.9. Electrochemical Impedance Spectroscopy (EIS)

Electrochemical Impedance Spectroscopy was performed on thin films deposited by the dip coating method to investigate the kinetics of the thin films . Nyquist plots of dip coating onto ozone treated FTO are shown in the figure. Inset shows the circuit used for fitting the EIS plot. EIS was done at 10 mV amplitude and the frequency changed between 100kHz – 10mHz.[62] For all the plots there is a high and low frequency region. In the high-frequency region, the intercept and at the real axis show the solution resistance (Rs) while the diameter of semi-circle represents the resistance offered by the interface between the electrode, electrolyte and the charges that transfer. [63]

The Rct value of treated FTO deposited sample for 0, 2 and 4 minutes of dip coating are 46.2 Ω, 43.4 Ω, and 17.6 Ω. The incomplete formation of semi-circles is an indication of negligible charge transfer. This decrease in resistance indicates the uniformity of NiO thin film and efficient charge transfer.
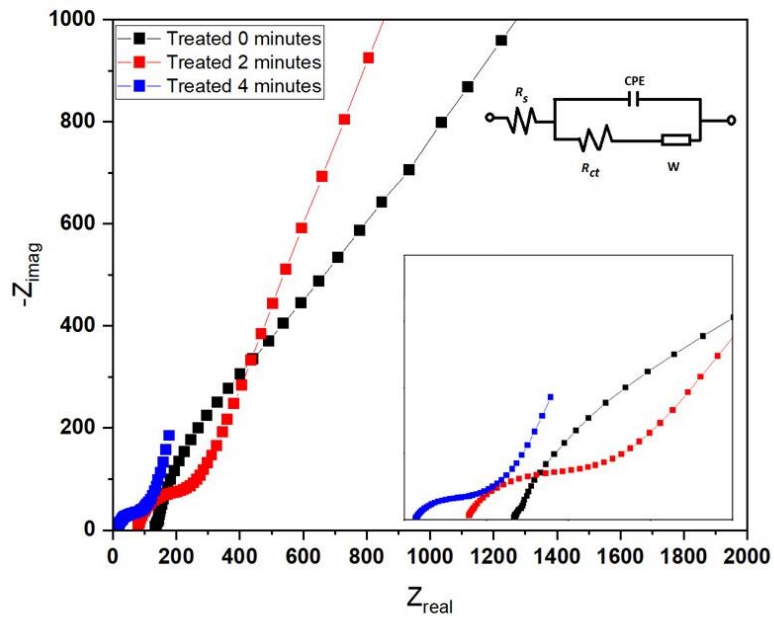
Figure 5. 17. Nyquist plots of NiO thin film on treated FTO samples, by dipping for 0, 2 and 4 minutes. Inset showing magnified plots.
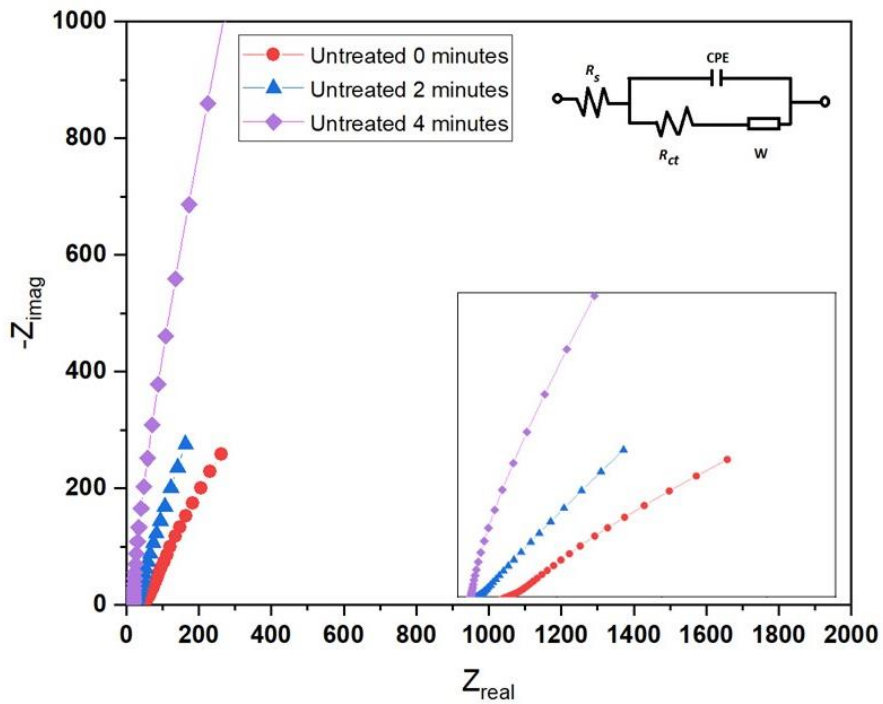
Figure 5. 18. Nyquist plots of NiO thin film on treated FTO samples, by dipping for 0, 2 and 4 minutes. Inset showing magnified plots.

The Rct value of untreated FTO deposited sample for 0, 2 and 4 minutes of dip coating are 48.92 Ω, 46.54 Ω, and 18.32 Ω. This decrease in resistance indicates the uniformity of NiO thin film and efficient charge transfer.

These results indicate that the resistance of treated samples is less than untreated samples relatively which confirms the increasing current values of the cyclic voltammetry. [64]

5.10. Hall Effect Measurements

The samples were prepared for hall effect measurements on clean glass substrates. These samples had been tested by the four-probe method. The following table shows the resistivity, conductivity, mobility, and Hall co-efficient of the untreated and treated FTO glass substrate coated with NiO thin films. These results were measured for dip coating samples as they were selected after other testing and characterization, proving to be the most stable, accurate in composition and uniformly deposited. The values for conductivity, resistivity, electron mobility and carrier concentration are shown in the table below. The increase in conductivity and decrease in resistivity suggests that these values are in alignment with the CV and EIS results. Moreover, the carrier concentration for treated samples increased that again confirms the high current values recorded for the same samples.

Table 3. Hall Effect Measurements of Dip Coating Samples

Sample name	Hall coefficient R_H (cm^3 /c)	Electrical conductivity σ (1/Ωcm)	Resistivity (kΩ cm)	Electron mobility (cm^2 /vs)	Carrier Concentration (x 10^{14}cm^{-3})
Untreated 0 mins	1.584×10^3	3.084	3.243	4.885	3.94
Untreated 2 mins	-1.327×10^4	5.946	1.682	7.894	4.702
Untreated 4 mins	-8.45×10^3	4.851	2.061	4.099	7.387
Treated 0 mins	7.63×10^7	1.65	6.046	8.192	1.260
Treated 2 mins	1.227×10^8	2.546	3.927	4.885	3.25
Treated 4 mins	8.405×10^7	8.793	1.137	3.370	1.629

Conclusion

Strong correlation was found between the film quality (related to morphology, optical properties and electrochemical properties of NiO films) and the plasma activation of FTO glass substrate. Similarly, the dipping time (before which the substrate is pulled out of the solution) also strongly influenced the film properties. The best coverage of NiO on top of FTO was achieved when using dip-coating technique (compared to spin coating and electrodeposition). Optical measurements reveal better transparency for plasma treated samples as their dipping time in NiO dispersion solution was increased. In addition, the NiO thin films showed improved reaction kinetics with increasing dipping time as revealed from cyclic voltammetry studies. Hall effect measurement results illustrated that all the NiO films exhibit p type conductivity which improved with increasing dipping time.

References

[1]   Al Mamun, A., et al., *Effect of hot-casted NiO hole transport layer on the performance of perovskite solar cells.* (2019). **188**: p. 609-618.

[2]   Soleimanpour, A.M., A.H.J.M.S. Jayatissa, and E. C, *Preparation of nanocrystalline nickel oxide thin films by sol–gel process for hydrogen sensor applications.* (2012). **32**(8): p. 2230-2234.

[3]   Xiang, L., X. Deng, and Y.J.S.M. Jin, *Experimental study on synthesis of NiO nano-particles.* (2002). **47**(4): p. 219-224.

[4]   Haider, A.J., et al., *Enhance preparation and characterization of nickel-oxide as self-cleaning surfaces.* (2019). **157**: p. 1328-1342.

[5]   Nalage, S., et al., *Sol–gel synthesis of nickel oxide thin films and their characterization.* (2012). **520**(15): p. 4835-4840.

[6]   Patil, P. and L.J.A.s.s. Kadam, *Preparation and characterization of spray pyrolyzed nickel oxide (NiO) thin films.* (2002). **199**(1-4): p. 211-221.

[7]   Cárdenas, A.A.B., *Synthesis and characterization of NiO for applications in photoelectronics devices.(2019)*

[8]   Zhou, K., et al., *The influence of crystallinity on the electrochromic properties and durability of NiO thin films.* (2017). **6**: p. 91-97.

[9]   Brioual, B., et al. *Electrochemical behavior of spray deposited nickel oxide (NiO) thin film in Alkaline electrolyte.* in *E3S Web of Conferences.* (2022). EDP Sciences.

[10]   Xia, X., et al., *Electrochromic properties of porous NiO thin films prepared by a chemical bath deposition.* (2008). **92**(6): p. 628-633.

[11]   Xia, X., et al., *Morphology effect on the electrochromic and electrochemical performances of NiO thin films.* (2008). **53**(18): p. 5721-5724.

[12]   Tong, B., M.J.E. Ichimura, and C.i. Japan, *Electrochemical Deposition of Transparent p-Type Semiconductor NiO.* (2018) **101**(2): p. 45-50.

[13]   Mouchou, R., et al., *Fabrication of p-NiO/n-TiO2 Solar Device for Photovoltaic Application.* (2021) p. 1-10.

[14]   Echresh, A., et al., *Optimization and characterization of NiO thin film and the influence of thickness on the electrical properties of n-ZnO nanorods/p-NiO heterojunction.* (2014) **29**(11): p. 115009.

[15]   Zhao, Y., et al., *Sputtering power induced physical property variation of nickel oxide films by radio frequency magnetron sputtering.* (2018). **21**.

[16]   Kaya, D., et al., *Investigation of optical, electronic, and magnetic properties of p-type NiO thin film on different substrates.* (2021). **732**: p. 138800.

[17]   Fakharpour, M. and M.H.J.A.P.A. Karimi Tafti, *Temperature and substrate effect on the electrical and structural properties of NiO columnar nanostructure.* (2023). **129**(3): p. 234.

[18]   Nishihara, Y., et al., *Influence of O2 plasma treatment on NiOx layer in perovskite solar cells.* (2018). **57**(4S): p. 04FS07.

[19]   Wang, T., et al., *Efficient inverted planar perovskite solar cells using ultraviolet/ozone-treated NiOx as the hole transport layer.* (2019). **3**(6): p. 1900045.

[20]   Napari, M., et al., *Nickel oxide thin films grown by chemical deposition techniques: Potential and challenges in next-generation rigid and flexible device applications.* (2021). **3**(5): p. 536-576.

[21]   Kaliyaperumal, A., et al. *Structural, Optical and Electrical Properties of Nanocrystalline Nickel Oxide Thin Films Prepared by Hydrothermal and Sol-Gel Methods.* in *IOP Conference Series: Materials Science and Engineering.* (2022). IOP Publishing.

[22]   Shuihab, A. and S. Khalf. *Fabrication and characterization of nickel oxide nanoparticles/silicon NiO NPS/Si.* in *AIP Conference Proceedings.* (2018). AIP Publishing.

[23]   Cai, C., et al., *Enhanced hole extraction by NiO nanoparticles in carbon-based perovskite solar cells.* (2019). **312**: p. 100-108.

[24]   Maaoui, B., et al., *Synthesis and characterization of physical properties of the NiO thin films by various concentrations.* (2020). **20**(3): p. 79-87.

[25]   Islam, M.B., et al., *NiO x hole transport layer for perovskite solar cells with improved stability and reproducibility.* (2017). **2**(5): p. 2291-2299.

[26]   Xu, L., et al., *Inverted perovskite solar cells employing doped NiO hole transport layers: A review.* (2019). **63**: p. 103860.

[27]   Steirer, K.X., et al., *Solution deposited NiO thin-films as hole transport layers in organic photovoltaics.* (2010). **11**(8): p. 1414-1418.

[28]   Lian, X., et al., *Polymer Modification on the NiO x Hole Transport Layer Boosts Open-Circuit Voltage to 1.19 V for Perovskite Solar Cells.* (2020). **12**(41): p. 46340-46347.

[29]   Zhao, P., et al., *Device simulation of inverted CH3NH3PbI3− xClx perovskite solar cells based on PCBM electron transport layer and NiO hole transport layer.* (2018). **169**: p. 11-18.

[30]   Seo, S., et al., *An ultra-thin, un-doped NiO hole transporting layer of highly efficient (16.4%) organic–inorganic hybrid perovskite solar cells.* (2016). **8**(22): p. 11403-11412.

[31]   Pae, S.R., et al., *Improving uniformity and reproducibility of hybrid perovskite solar cells via a low-temperature vacuum deposition process for NiO x hole transport layers.* (2018). **10**(1): p. 534-540.

[32]   Caruge, J.-M., et al., *NiO as an inorganic hole-transporting layer in quantum-dot light-emitting devices.* (2006). **6**(12): p. 2991-2994.

[33]   Hu, Z., et al., *Sol-gel-processed yttrium-doped NiO as hole transport layer in inverted perovskite solar cells for enhanced performance.* (2018). **441**: p. 258-264.

[34]   Wu, W.-Q., et al., *Molecular doping enabled scalable blading of efficient hole-transport-layer-free perovskite solar cells.* (2018). **9**(1): p. 1-8.

[35]   Yao, Y., et al., *Organic hole-transport layers for efficient, stable, and scalable inverted perovskite solar cells.* (2022). **34**(44): p. 2203794.

[36]   Bag, A., et al., *Effect of absorber layer, hole transport layer thicknesses, and its doping density on the performance of perovskite solar cells by device simulation.* (2020). **196**: p. 177-182.

[37]   Kim, G.-W., D.V. Shinde, and T.J.R.a. Park, *Thickness of the hole transport layer in perovskite solar cells: performance versus reproducibility.* (2015). **5**(120): p. 99356-99360.

[38]   Lin, X., et al., *Efficiency progress of inverted perovskite solar cells.* (2020). **13**(11): p. 3823-3847.

[39]   Liu, T., et al., *Inverted perovskite solar cells: progresses and perspectives.* (2016). **6**(17): p. 1600457.

[40]   Said, A.A., J. Xie, and Q.J.S. Zhang, *Recent progress in organic electron transport materials in inverted perovskite solar cells.* (2019). **15**(27): p. 1900854.

[41]   Wu, C.-G., et al., *High efficiency stable inverted perovskite solar cells without current hysteresis.* (2015). **8**(9): p. 2725-2733.

[42]   Li, B. and W.J.C.m. Zhang, *Improving the stability of inverted perovskite solar cells towards commercialization.* (2022). **3**(1): p. 65.

[43]   Ul-Hamid, A., *A beginners' guide to scanning electron microscopy.* Vol. 1. (2018): Springer.

[44]   Chen, W., et al., *Understanding the doping effect on NiO: toward high-performance inverted perovskite solar cells.* (2018). **8**(19): p. 1703519.

[45]   Lloyd, M.T., et al., *Influence of the hole-transport layer on the initial behavior and lifetime of inverted organic photovoltaics.* (2011). **95**(5): p. 1382-1388.

46.   Mourdikoudis, S., R.M. Pallares, and N.T.J.N. Thanh, *Characterization techniques for nanoparticles: comparison and complementarity upon studying nanoparticle properties.* (2018). **10**(27): p. 12871-12934.

[47]   Zhang, S., L. Li, and A. Kumar, *Materials characterization techniques.* (2008): CRC press.

[48]   Titus, D., E.J.J. Samuel, and S.M. Roopan, *Nanoparticle characterization techniques*, in *Green synthesis, characterization and applications of nanoparticles.* (2019), Elsevier. p. 303-319.

[49]   Hamidon, T.S., et al., *Potential of zinc based-graphene oxide composite coatings on mild steel in acidic solution.* (2021). **98**(12): p. 100243.

[50]   Abou-Ras, D., T. Kirchartz, and U. Rau, *Advanced characterization techniques for thin film solar cells*. Vol. 2. (2011): Wiley Online Library.

[51]   De la Torre, J., et al., *Using silicon nanostructures for the improvement of silicon solar cells' efficiency.* (2006). **511**: p. 163-166.

[52]   Zeng, L., et al., *Efficiency enhancement in Si solar cells by textured photonic crystal back reflector.* (2006). **89**(11).